

PROTON PRECESSION MAGNETOMETER

Arefin Islam Ayon

Bachelor of Engineering
Electronic Engineering Major



Department of Electronic Engineering
Macquarie University

September,04 2017

Supervisor: Professor Yves De Deene



ACKNOWLEDGMENTS


I would like to acknowledge the help of my academic supervisor Professor Yves De Deene for guiding me. I would also like to thank Morgan Wheatly who is a Masters student working under Yves. Morgan showed me some of the lab procedures that I had to carry out during the etching process. This thesis work is aimed to design a prototype of a Proton Precession Magnetometer. This prototype will be used to measure the Earth's magnetic field which is its primary goal but later on it will be further transformed to a portable MRI device. The stages to its design will be further explained throughout my paper.



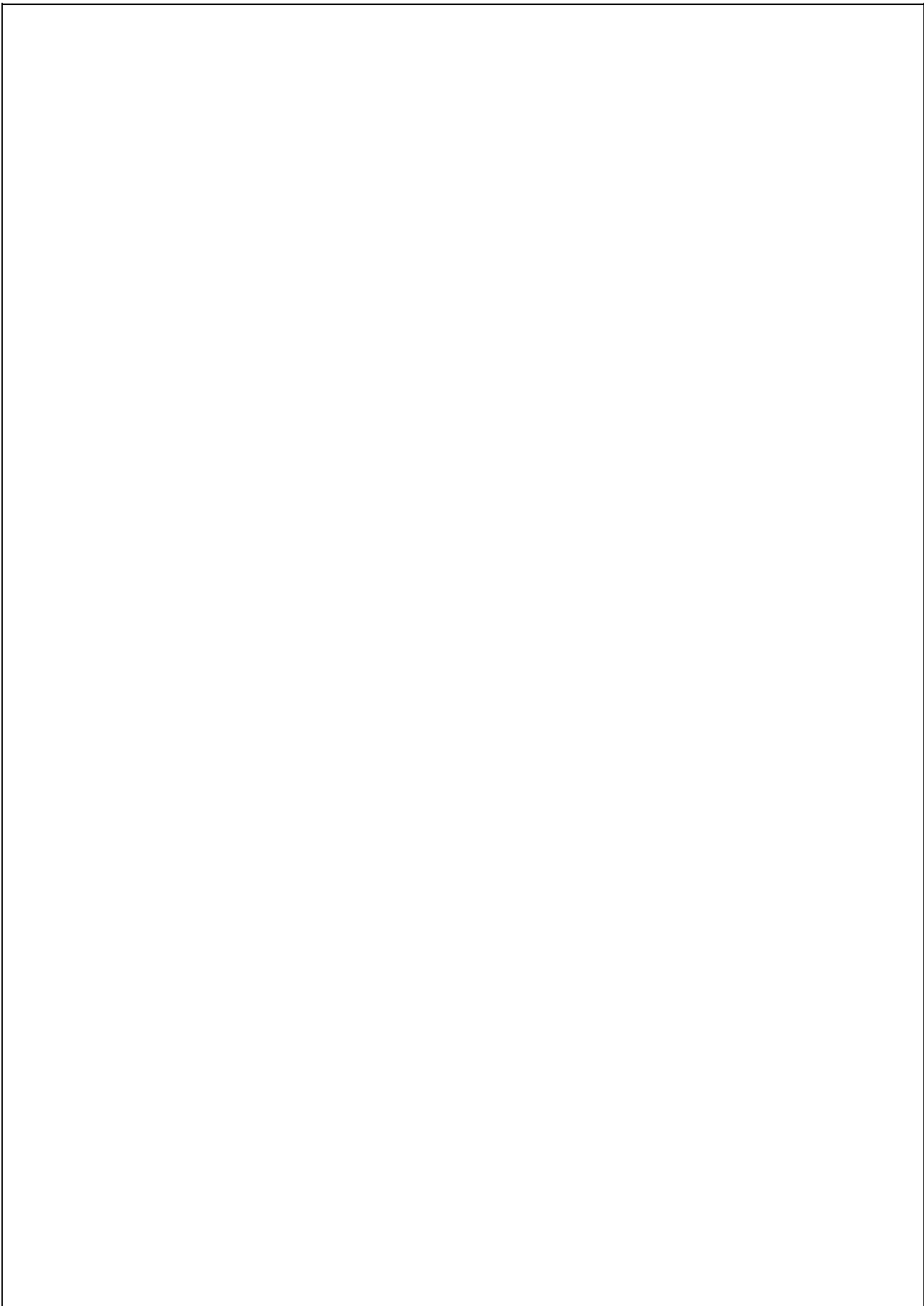
STATEMENT OF CANDIDATE

I, Arefin Islam Ayon, declare that this report, submitted as part of the requirement for the award of Bachelor of Engineering in the Department of Electronic Engineering, Macquarie University, is entirely my own work unless otherwise referenced or acknowledged. This document has not been submitted for qualification or assessment at any academic institution.

Student's Name: Arefin Islam Ayon

Student's Signature: 

Date: **13/11/17**



ABSTRACT

Magnetic resonance imaging (MRI) is a medical imaging technique to produce images of an anatomy and the physiological process of the body. MRI devices use very strong magnetic fields and radio waves to process these images of human body. MRI is based on the physical principle of Nuclear Magnetic Resonance (NMR) . This is a phenomenon where an atom nucleus placed in an external magnetic field absorbs and emits radio frequency . The cost of a conventional clinical MRI scanner is in the order of 2-3 million dollars and additional maintenance and operating costs make that a single MRI exam in the order of the \$1000 dollars. Also sometimes the MRI of the entire body is not required. From this originates the idea of this project which is to prototype a proton precision magnetometer (PPM) which will lead us to explore the possibilities for cheaper MRI technology. This magnetometer will be first prototyped to measure earth's magnetic field but in longer term it can be further extended for other industrial and biomedical applications. Similar to clinical MRI, PPM relies on the signal from precessing nuclear magnetic dipoles. The frequency of the precession is directly proportional to the external magnetic field strength. And when there are enough precessing protons resulting an oscillating magnetic field will be created. This frequency of this generated oscillating field is exactly what we will be measuring with the PPM which will correspond to Earth's magnetic field.



Contents

Acknowledgments	iii
Abstract	vii
Table of Contents	ix
List of Figures	xi
List of Tables	xiii
1 Introduction	1
1.1 History of Magnetometer	1
1.2 Measurement of the Field	1
1.3 Project Goal	2
1.4 Overview of the PPM	3
2 Background and Related Work	5
2.1 Literature Review	5
2.1.1 The low cost Proton Precession Magnetometer developed at the Indian Institute of Geomagnetism	6
2.1.2 The analysis of the polarization circuit to Proton precession mag- netometer	6
2.1.3 Active Magnetic Field Compensation System Using Proton Preces- sion Scalar Magnetometer for SQUID based applications	9
2.1.4 A high precession Proton Magnetometer Based on a Multi-Channel frequency Measurement	10
3 Requirements and experimental procedures	13
3.1 Polarization Coil and platform	13
3.1.1 PPM positioning Information	13
3.1.2 Wire for the polarization coil	13
3.1.3 Polarization Coil Construction	14
3.1.4 Polarization Coil specifications	14
3.1.5 Polarization Coil Platform	14

3.1.6	Magnetic Field Strength produced by the Coil	15
3.2	Pulse Controller	16
3.2.1	Advantages of using MOSFETs	16
3.2.2	Pulse Controller Circuit description	17
3.3	Sensor Coil	20
3.3.1	Sensor Coil Requirements	20
3.3.2	Sensor coil specification	21
3.3.3	Choosing the correct wire and Construction of the Sensor coils . . .	21
3.4	Amplifier	22
3.4.1	Advantage of Differential Amplifier	23
3.4.2	Providing power to the Amplifier	24
3.4.3	Tuning to the Correct Capacitor Value	25
3.5	Data Acquisition Process	27
3.5.1	Sampling Rate and resolution	27
4	Results and Discussions	29
4.1	Results	29
4.2	Discussions	32
4.2.1	Noisy Signal	32
5	Conclusions and Future Work	35
5.1	Conclusions	35
5.1.1	Future Work	35
	Index	35
A	Data sheets of components used in the circuit	37
A.1	Datasheet of MOSFET used for the polarization circuit	37
A.2	Optocoupler Data sheet	46
A.3	Instrumentational Amplifier and op amp datasheet	54
B	Project attendance form	69
B.1	Overview	69
	Bibliography	71

List of Figures

1.1	System Overview of PPM	3
2.1	polarization, excitation of sample and signal detection sequence	6
2.2	Block diagram of Earth's Field NMR system	7
2.3	Precession of a proton	8
2.4	Polarization circuit	8
2.5	Experimental 1-D Helmholtz setup [1]	9
2.6	Precession Signal with enhanced SNR [1]	10
2.7	Hardware design of magnetometer based on multi-channel frequency measurement [2]	11
2.8	Working sequence of the instrument [2]	11
3.1	Polarization Coil Platform	15
3.2	Example of a P-channel enhancement type MOSFET	17
3.3	Schematic of the pulse controller	18
3.4	PCB design of the pulse controller	19
3.5	Sensor coils wire direction [3]	22
3.6	Amplifier Circuit Schematic	23
3.7	Sensor inputs to the Amplifier	23
3.8	Amplifier PCB	24
3.9	Capacitance in Parallel	26
3.10	Arduino Code	28
4.1	Polarization coil housing two sensor coils	29
4.2	Amplifier and the Polarization circuit	30
4.3	Raw data with noise	31
4.4	Running sequence	32
4.5	Amplifier summing circuit	33
4.6	Shifting of the signal	34



List of Tables



Chapter 1

Introduction

1.1 History of Magnetometer

Magnetometer is an instrument for measuring the direction and the strength of magnetic fields. Magnetometers are also sometimes used in calibration of electromagnets and permanent magnets and also to determine the magnetization of materials. The first simplest absolute magnetometer was invented by C.F Gauss in 1832. [4]. The design consisted of a permanent bar magnet suspended horizontally by a gold fiber.

1.2 Measurement of the Field

Magnetic fields can be measured in various ways. The simplest measurement technique still applied today which makes the use of regular compass which consists of a permanently magnetized needle that is balanced onto a pivot in the horizontal plane. The magnetized needle aligns itself exactly along the magnetic field vector when there is a presence of magnetic field and in the absence of gravity. But when it is balanced onto a pivot in the presence of gravity, the needle aligns itself along the horizontal component of the field. A magnetized needle can also be pivoted and balanced about a horizontal axis. Similarly, a device called dip meter is first aligned in the direction of the magnetic meridian as defined by a compass, the needle lines up with the total field vector and measures the inclination angle. Finally it becomes possible to measure the magnitude of the horizontal field by the oscillations of the compass needle.

On the other hand, magnetic observatories measures and records the earth's magnetic field from different locations. The technique that this observatories uses as said in the article [4] are magnetized needles with reflecting mirrors that are suspended by quartz fibers. Then the light beams that are reflected from the mirrors are imaged on a photographic negative which is attached on a rotating drum. Variations in the magnetic field causes corresponding deflections on the negative. Then the print in the negative is used which is called the magneto-gram to measure the magnetic field [4]. This technique to record the data of the field has been used for hundreds of years until recent times.

In recent times, older instruments are being gradually replaced by new convenient methods of measuring magnetic fields. One such method involves the proton precession magnetometer. This technique uses the magnetic and gyroscopic properties of protons in a hydrogen rich fluid such as water. In this technique, the magnetic moments of the proton in the fluid are first aligned by a strong magnetic field produced by a polarization coil. The magnetic field is then turned off abruptly, following that the protons try to align themselves with the earth's magnetic field. However, as the protons are spinning and also that they are magnetized, they precess around the earth's field with a frequency dependent on the magnitude of the latter. After that the sensor coil senses a weak voltage induced by the precession.

1.3 Project Goal

Magnetic resonance imaging (MRI) is a medical imaging technique to produce images of an anatomy and the physiological process of the body. MRI devices use very strong magnetic fields and radio waves to process these images of human body. MRI is based on the physical principle of Nuclear Magnetic Resonance (NMR). This is a phenomenon where an atom nucleus placed in an external magnetic field absorbs and emits radio frequency. In conventional MRI, hydrogen atoms are often used as they are naturally occurring in the human body in abundance particularly in water and fat. MRI in clinical practice are conducted in large MRI scanners where a large magnetic field is created by use of superconducting magnets. The cost of a conventional clinical MRI scanner is in the order of 2-3 million dollars and additional maintenance and operating costs make that a single MRI exam in the order of the \$1000 dollars. Also sometimes the MRI of the entire body is not required. From this originates the idea of this project which is to prototype a proton precision magnetometer (PPM) which will lead us to explore the possibilities for cheaper MRI technology. This magnetometer will be first prototyped to measure earth's magnetic field but in longer term it can be further extended for other industrial and biomedical applications. Similar to clinical MRI, PPM relies on the signal from precessing nuclear magnetic dipoles. The prototype PPM will acquire a NMR signal in a sample of water in the earth's magnetic field. It basically takes advantage of the idea that protons have an intrinsic magnetic field much like of very small magnets. Similar to the MRI example discussed above the direction of the proton's field will precess (rotate) around the applied external magnetic field. The frequency of the precession is directly proportional to the external magnetic field strength. And when there are enough precessing protons resulting an oscillating magnetic field will be created. This frequency of this generated oscillating field is exactly what we will be measuring with the PPM. As the precession frequency of the protons are proportional to the magnetic field strength, the frequency of the precessing protons measured with the PPM provides an accurate measure of the Earth magnetic field.

1.4 Overview of the PPM

Firstly a general description of how the PPM actually works. We begin by selecting our sample which is a hydrogen rich substance such as water. We place about two ounces of water inside a cylindrical tube. The tube is then placed inside the sample coil which is then placed inside the polarization coil. Then a field is generated by the polarization coil which then polarizes the sample for a period of time. After the polarization coil is switched off, the signals generated by the precessing protons in the sample is then recorded by the data acquisition system. Then a spectrum is produced by processing the digitized signal using "Arduino" and "Matlab" which then gives the precession frequency of the protons.

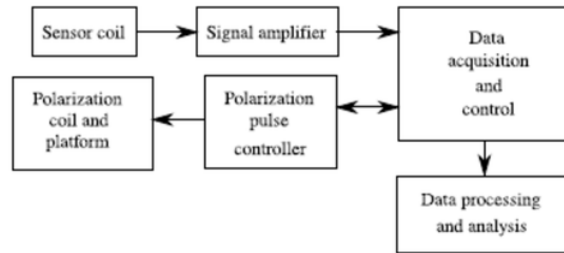


Figure 1.1: System Overview of PPM

[3]

A general overview of the total system is shown in figure 1.1. The PPM can be divided into three parts: the polarization system, the sensor system and the data acquisition system.

Now we start with the polarization system. The purpose of the polarization system is to generate a large magnetic field compared to the Earth's and also in a direction perpendicular to the Earth's field. To make the two fields perpendicular to each other, we mount the polarization coil on a tilt able platform. The polarization coil needs to be capable of being turned on for a specific period of time and then turned off swiftly. To make this possible we designed a polarization pulse controller. The pulse controller design and schematics have been taken from a design which was already made before from the book 'Signals from the subatomic world: How to build a proton precession magnetometer' by Stefan Hollos and Richard Hollos [3]. In that previous design they used 'AT90S2313' micro controller but in our design we will be using an Arduino instead. The reason an Arduino has been chosen over a regular micro-controller is because micro-controllers are typically preprogrammed before being soldered into the PCB and it is unchangeable where as using an Arduino makes it all easy as it can be programed by using C or C++. Moreover the Arduino is used as a plug and play device in corresponding to our Pulse Controller which makes our Pulse Controller design much simpler. Once programmed, to start the polarization process the Arduino or the Pulse controller waits for a signal from

the computer. The polarization process is mainly composed of turning on the current to the polarization coil for a significant period of time and the turning off instantaneously and then it signals the data acquisition system to start recording data.

The sensor consists of mainly two parts, the sample coil and the amplifier. The sample coil again is consisted of two identical coils side by side. One sample coil houses the hydrogen rich sample and its purpose is to inductively detect the very small magnetic field produced by the polarized protons that precess about the earth's magnetic field. The other sample coil is not there to house any sample but its purpose is to cancel out environmental magnetic fields. As mentioned before that the magnetic field produced by the polarized protons is very small and weak and thus to boost the signal into a detectable spectrum the sample coil needs to be connected and tuned by using capacitors to form a resonant circuit at the proton precession frequency [3]. To overcome this problem the amplifier has been designed which has a bank of capacitors that can be used to tune the sample coil. The amplifier design has been taken from the same book mentioned above and the design has not been altered as the gain will be by a factor of approximately 3.8 million which makes the amplifier a very sensitive part of the whole system.

The last part is the data acquisition and control system. It consists of a computer with an Arduino which controls the pulse controller and then receives the amplified signal from the amplifier which is then represented by using 'Arduino IDE' and 'MATLAB'.

Chapter 2

Background and Related Work

2.1 Literature Review

The measurement of molecular motion using pulsed magnetic field gradients in combination with nuclear magnetic resonance (NMR) spin echoes has been widely applied in materials science under laboratory conditions. In the article [5] it describes about an earths field nuclear magnetic resonance apparatus which can be used to carry out pulsed gradient spin echo (PGSE) diffusion measurements of self-diffusion under Antarctic conditions. The device is portable and incorporates automated process control allowing direct measurements of the Larmor precession. The article further describes that for accurate signal averaging how the system uses clock for pulse sequencing, excitation pulse synthesis and detection. We are using similar clock for pulse sequencing technique in our pulse controller design.

The method that is used to carry out experiments through this system is, to polarize a sample by simple electro magnet and then allowing detection to take place. The sample is placed in the center of the polarizing coil which is driven by an amplifier. According to the article [5] the magnetic field produces a net magnetization in the sample almost orthogonal to the direction of the earths magnetic field. The polarizing coil then excites the sample which is then received by the receiver coil which is then passed through an amplifier to enhance the received signal as it is very small in scale. The overall process has been showed in figure 2.1.

A detailed overview of the earths magnetic NMR system has been shown in figure 2.2. It shows that the system uses a polarizing coil to excite the sample which is placed in the center of that coil. It has a receiver coil which receives the signal which is then passed through an amplifier to enhance that small received signal which is then sent to data acquisition process.

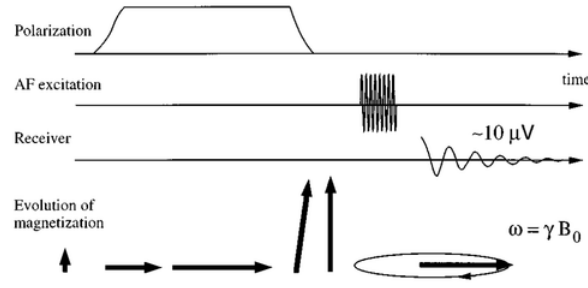


Figure 2.1: polarization, excitation of sample and signal detection sequence [5]

2.1.1 The low cost Proton Precession Magnetometer developed at the Indian Institute of Geomagnetism

Another article that is about the low cost Proton Precession Magnetometer developed at the Indian Institute of Geomagnetism. The system is called the PM7 [6]. It utilizes the precession of the spinning protons or nuclei of the hydrogen atoms in a sample of Hexane to measure the total magnetic density. The spinning protons in this sample are temporarily aligned or polarized by uniform magnetic field produced by passing a current through the coil. When most of the protons are aligned in the direction of the generated magnetic field the current is switched off and the spin of the proton causes them to precess about the direction of the Earth's magnetic field. Those precessing protons generate a small signal in the same coil which is used to polarize them whose frequency is precisely proportional to the total magnetic field.

2.1.2 The analysis of the polarization circuit to Proton precession magnetometer

A journal which has been published in "2012 International conference on industrial control and Electronics Engineering" showed an analysis of the polarization circuit which is used to control the current in the polarizing coil. The journal is mainly divided into three main parts. The first part describes the principle of proton precession magnetometer which we have already covered before. In the second part they showed and explained the equation of the polarization current and the time constant. And in the last part they showed the effects of the attenuation of the coil current which includes the schematic diagram of the linear attenuation and the nonlinear attenuation.

At first the journal confirms the significance of the polarizing circuit on the proton precession magnetometer. It also explains that the hydrogen proton produces magnetic

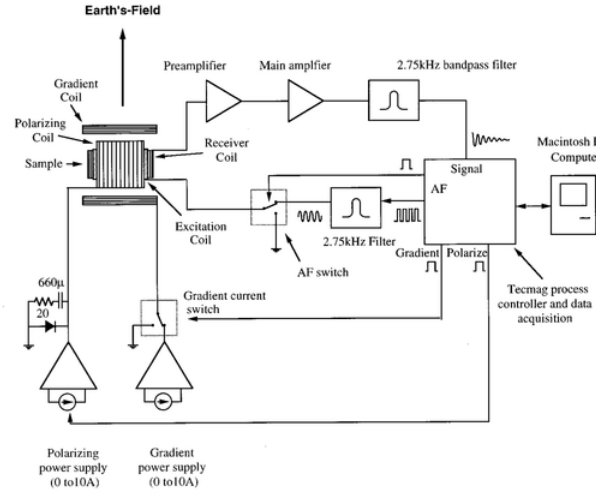


Figure 2.2: Block diagram of Earth's Field NMR system [5]

moment due to the spin [7]. As described in the journal, that under the influence of the generated or external magnetic field that is perpendicular to the geomagnetic field, this causes a change in the direction of the hydrogen proton magnetic moment which is equal to the external magnetic fields, and this process is called polarization as discussed earlier. After the external magnetic field disappears, the hydrogen proton magnetic moment will try to move towards the geomagnetic field \mathbf{T} . Thus this behavior of the proton is called the proton precession. The paper also includes a physics theory that shows that the angular velocity of the proton precession ω is proportional to the geomagnetic field \mathbf{T} [7]. The relationship is shown in equation 2.1. This equation is also known as the LARMOR equation and the γ_p is the gyro-magnetic ratio. The proton precession is also shown in figure 2.3.

$$\omega = \gamma_p \cdot \mathbf{T} \quad (2.1)$$

The polarization circuit of the proton precession magnetometer

Figure 2.4 shows a circuit that has been used in this journal [7] to deduce some current and time equations. The paper says that HEXFET or also known as power MOSFETs are best for switching the polarizing current as they have much lower on resistance that the loss through them will be negligible. They also have a large reverse breakdown voltage of the drain to source. We are also using this type of MOSFET's in our design and instead of one we are using 8 of them which is explained latter in the report. Figure 2.4 relates to the equation in 2.2. It shows that a certain voltage V_{cc} is applied in the circuit as polarizing

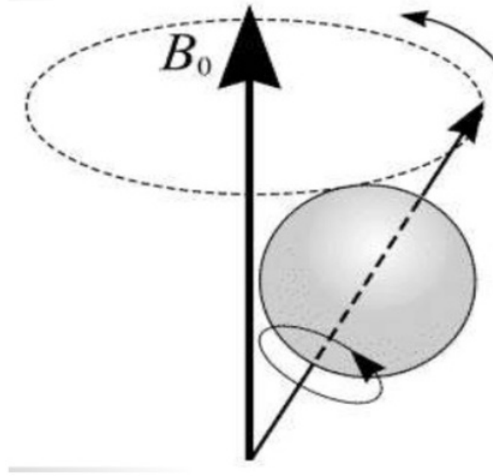


Figure 2.3: Precession of a proton

supply for the magnetometer and when the current passes through the MOSFET the coil is charged. Then according to the diagram that they showed, the L and R form a series circuit. And when the current is ON, then the polarization current behaves as an index curve which is given by the equation in 2.2. The time constant τ is calculated as shown in the equation 2.3 and the polarization current maintains the stability when the time is more than 5τ .

$$I(t) = I_0(1 - \exp^{-t/\tau}) \quad (2.2)$$

$$\tau = L/R \quad (2.3)$$

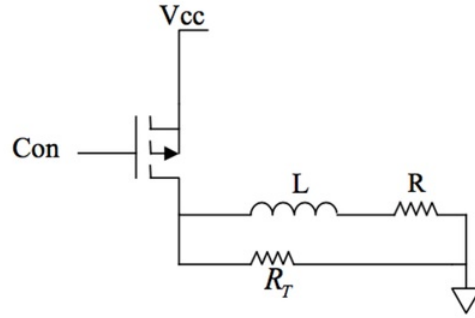


Figure 2.4: Polarization circuit

2.1.3 Active Magnetic Field Compensation System Using Proton Precession Scalar Magnetometer for SQUID based applications

This journal has been published on 2015 on ICEE. They focused on active compensation of magnetic fields for the establishment of a silent environment for SQUID applications. All this applications were done by implementing a sensitive proton precession scalar magnetometer. They used the proton precession scalar magnetometer to measure external magnetic field and based on the measured signal they used other processing and amplification circuits to provide the compensated current in the coil. The readout circuits that they used to measure the precession frequency of hydrogen atoms have been designed with special noise consideration to increase SNR (Signal to Noise ratio) for maximum sensitivity [1].

Low Noise Experimental Setup

Figure 2.5 is the experimental setup that they used for low noise experiments of the Proton Precession Magnetometers. By using this they investigated the effect of different measurement parameters. Figure 2.6 is their obtained precession signal of the Earth's field which they measured in outdoor places. As shown in figure 2.6, they proved that they managed to increase the SNR significantly by optimizing the sensor parameter and reduction of the system and intrinsic noises. By doing so they eventually achieved the SNR to be 150 for the precession signal in the noisy city condition [1].

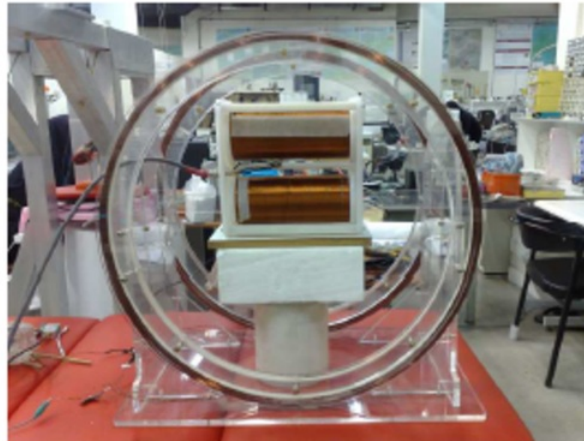


Figure 2.5: Experimental 1-D Helmholtz setup [1]

To get a higher amplitude signal, they updated the design by increasing the polarization signal from 10mT to 23mT. They also increased the volume of the sample i.e hydrogen proton rich liquid and increased the number of turn in the coils. Another change they

made to increase the sensitivity to the receiving signal is by widening the coil structure and reduced the thermal noise by increasing the diameter of the coil wires.

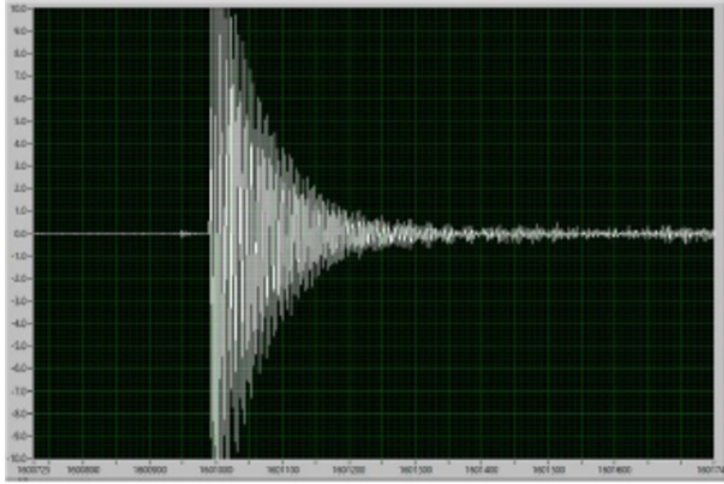


Figure 2.6: Precession Signal with enhanced SNR [1]

2.1.4 A high precession Proton Magnetometer Based on a Multi-Channel frequency Measurement

This journal mainly focused to improve the precision and the anti-interference ability of a traditional proton precession magnetometer. The designed that they proposed was based on a multi-channel frequency measurement [2]. This paper discusses the principle of the Larmor precession effect and gives a detailed explanation regarding the signal disposal system and the multi channel frequency measurement algorithm of the device. At last they compared their multi channel frequency measurement based magnetometer to the commercial Overhauser magnetometer by runnings experiments and tests between them in outdoor conditions. The tests results showed that the performance of their instrument is close to the commercial ones. None the less, their proposed design has the advantage of convenience for field operation, strong anti interference and high field magnetic measurement precision. This proves the effectiveness of the multi-channel frequency measurement based magnetometers under weak magnetic measurement conditions.

Design of their proposed instrument

The proposed hardware design of the instrument is shown in figure 2.7. When the instrument is turned on, then the DC excitation system generates a DC pulse [2] to excite the sensor to collect the Larmor Precession signal. Secondly, after the excitation process, the

tuned capacitors extracts the signal after which the signal conditioning system also known as amplifier system will amplify the received signal and transforms it into a square wave.

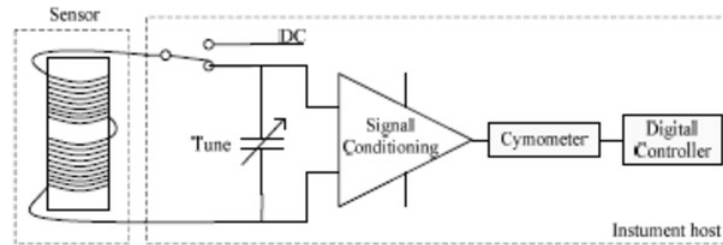


Figure 2.7: Hardware design of magnetometer based on multi-channel frequency measurement [2]

After that the cymometer finishes the frequency measurement. The figure 2.8 shows the overall process that occurs.

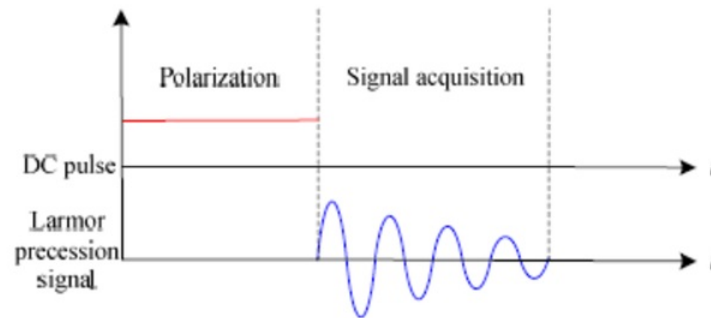


Figure 2.8: Working sequence of the instrument [2]

Chapter 3

Requirements and experimental procedures

3.1 Polarization Coil and platform

The main purpose of the polarization coil is to create a magnetic field greater than the earth's so that all the protons in the water which we will be using as our sample start precessing about the field produced by the coil and not the earth's field. For this reason, the field produced by the polarization coil does not need to be uniform, as long as it is large compared to the Earth's field.

3.1.1 PPM positioning Information

The axis around which the polarization coil is wound should be oriented in a way so that it is perpendicular to the Earth's magnetic field direction. In the northern hemisphere, the magnetic field entering the ground has an angle which is called the magnetic inclination angle. Therefore the polarization coil must be tilted from the horizontal plane at an angle equal to the magnetic inclination angle of the Earth.

3.1.2 Wire for the polarization coil

To polarize the sample it is necessary to send a large amount of current through the polarizing coil which is approximately 10amps. Therefore the wire of the polarization coil must be large enough to handle this much current. Keeping that in mind we used 14 gauge enameled magnet copper wire which is wound around an acrylic tube. The pulse controller turns off the approximated 10amps of current very quickly in about 200-300 milliseconds. This quick switching off process induces a very large voltage of about 270 Volts. Thus confirming the voltage rating of the wire used for the polarization coil will save the system from failure.

3.1.3 Polarization Coil Construction

The polarization coil is made of three parts. The design consists of three parts which includes an acrylic extruded clear tube of outer diameter of 110mm and an inner diameter of 105mm. The other two parts are the two end pieces which are squares with a semi circle in one of the sides. The two end pieces need to have a circular hole of 110.5mm so that they fit on the both sides of the 100mm acrylic tube. The two end pieces are attached to the tube by using acrylic solvents but in our case we used $CHCl_3$ (Chloroform) as chloroform makes a strong seamless bond between acrylics. After that the coiling process was completed by winding wire around the tube manually. The number of coil layers made on the tube is 5 and each layer was coated with epoxy resin before winding the next layer. This epoxy coating prevents the winding from coming undone. This coating also makes the coil more mechanically stable.

3.1.4 Polarization Coil specifications

- 14 AWG enameled copper magnet wire, diameter (w/o insul)=1.63mm
- coil inner diameter=105mm
- coil length=10cm
- number of layers=5
- turns per layer =56, total number of turns=280
- approximate resistance=1.3 ohm

3.1.5 Polarization Coil Platform

The position of the polarization coil needs to be oriented in a way so that it is perpendicular to the Earth's magnetic field. Also the magnetic field in the northern hemisphere of the earth's enters the ground at a certain angle which is known as magnetic inclination of the earth [3]. Therefore the polarization coil is required to be tilted from the horizontal by an angle equal to the magnetic inclination. To make this possible we need to mount the polarization coil on a tilt-able platform and then adjust the angle. The magnetic inclination angle varies from place to place which is why we found out our local magnetic inclination angle which is an approximate of $64^\circ 13'$. It can be easily calculated by putting the location that is the longitude and latitude in this website "<http://www.magnetic-declination.com/>".

The information that we got from the website is

- Latitude: $33^\circ 46' 23.3''$ S
- Longitude: $151^\circ 7' 1.7''$ E

- Magnetic declination: $+12^{\circ} 31'$
- Declination is POSITIVE (EAST)
- Inclination: $64^{\circ} 13'$
- Magnetic field strength: 57024.0 nT

To make the platform, we used an acrylic sheet where the coil is mounted on. The sheet is then mounted on two triangular slopes which makes an angle of 64.5° with the horizontal plane. And then the whole construction is then glued using Araldite on a flat wooden sheet. Platform design has been shown in figure 3.1.

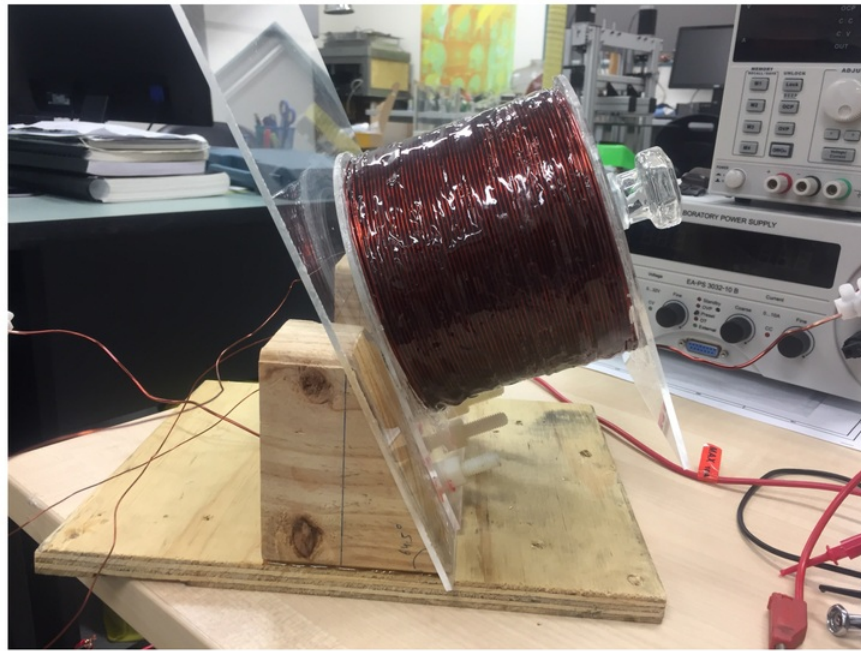


Figure 3.1: Polarization Coil Platform

3.1.6 Magnetic Field Strength produced by the Coil

The part of the design has an important aspect which needs to be considered before completing the design, which is the approximate magnetic field strength that will be produced by the polarization coil. The magnetic field strength is very crucial because one should know that the produced magnetic field by the coil is sufficient enough to polarize the

hydrogen proton or to get a proton precession signal. Thus to overcome this issue we used the equation 3.1 to make an approximate calculation.

$$B(x) = \frac{\mu I n^2}{2} \left[\left(\frac{h}{2} - x \right) \ln(a(x)) + \left(\frac{h}{2} + x \right) \ln(b(x)) \right] \quad (3.1)$$

Equation 3.1 is used to measure the magnetic field where B represents magnetic field, x is the distance from the geometric center of the coil.

3.2 Pulse Controller

As discussed above, the pulse controller is used to turn the current on and off in the polarization coil. Time required to turn on the current is not as important as time taken turning off the current. This is because, to get a good precession signal the current in the polarization coil needs to be turned off very fast or else if it happens the other way, then the proton magnetic moments will just slowly follow the field ending up with no precession signal. There are many ways to overcome this problem. The first solution is a mechanical relay. But using a mechanical relay can arise several issues. Firstly, a mechanical relay has a very short lifetime compared to a solid state switching devices such as transistors. In our design the current will be switched on and off so many times that the mechanical relay will fail more quickly. A relay is just similar to a normal switch. Another problem with this is the possibility of electric arcing across the contacts while switching which happens due to the large voltage induced in the coil when the current is turned off. The solution to this problem can be solved by using semiconductor power devices such as power MOSFET.

3.2.1 Advantages of using MOSFETs

The type of MOSFET that we will be using in our pulse controller for our Proton Precession Magnetometer is P-Channel enhancement type. It is a solid state switch which has three terminals called the source, drain and gate.

A schematic of a MOSFET has been shown in figure 3.1. The gate voltage controls the source to drain current flow of the device. As shown in the figure above, the P-Channel MOSFET requires (-)ve negative voltage in the gate to source terminal to allow the source to drain current flow. The lower the gate voltage is with respect to the source voltage, the more the current flows through the device up to a certain limit. The MOSFETs have a maximum limit of -20 volts from the gate to source terminal. The amount of current flows through this type of devices are also limited. Another important fact about this device is the drain to source breakdown voltage. At this breakdown voltage current will still flow through the device even if it is in the off state. This phenomenon is quite similar to the electrical arcing issue that occurs in mechanical switches when the voltage between the contacts gets too high.

But, it is important to notice that this limiting factor of MOSFET only arises when a single MOSFET is used. Fortunately some of this limitation problems can be eliminated by using several of this MOSFET together. By doing so, it is possible to increase the effective

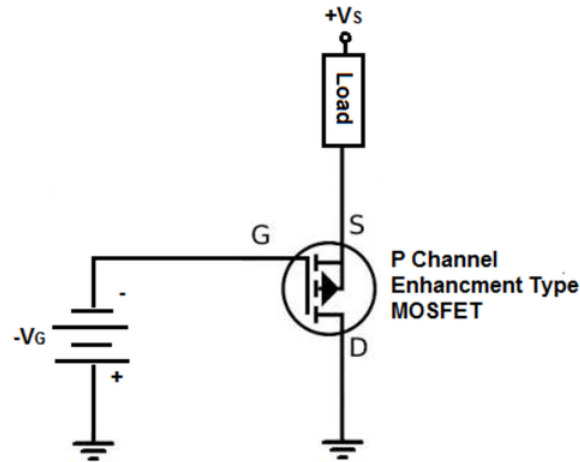


Figure 3.2: Example of a P-channel enhancement type MOSFET [8]

drain to source breakdown voltage. If we put two of the MOSFET in series then it will double the break down voltage. However, a problem with this is that there will always be a voltage drop for which there will be some finite resistance when there is a current flow through the MOSFET. This finite resistance is called the ON-resistance and if we put two resistance in series then we just double the ON-resistance [3]. To solve this problem we use our knowledge from elementary circuit theory where we know that by putting two equal value of resistors in parallel will result in an equivalent resistance of half the value. By using the theory we use a parallel combination of two MOSFETs in series for a total of four MOSFETs to solve our problem of doubling the break down voltage without increasing or doubling the ON-resistance.

3.2.2 Pulse Controller Circuit description

The schematic of the pulse controller circuit is shown in figure 3.2. The design has four MOSFETs in series that are placed in two parallel combinations. By arranging the MOSFETs in this way decreases the ON-resistance by three-fourths and gives an effective ON-resistance of one fourth of a single MOSFET. Again by putting two of these parallel combinations in series will eventually result in a total effective resistance of one half the ON-resistance of a single MOSFET.

This arrangement of the MOSFET will also double the effective breakdown voltage. And the MOSFET that we will be using in our design is IRF6215. Each of the IRF6215 MOSFET has an effective ON-resistance of 0.3 Ohms and a minimum break down volt-

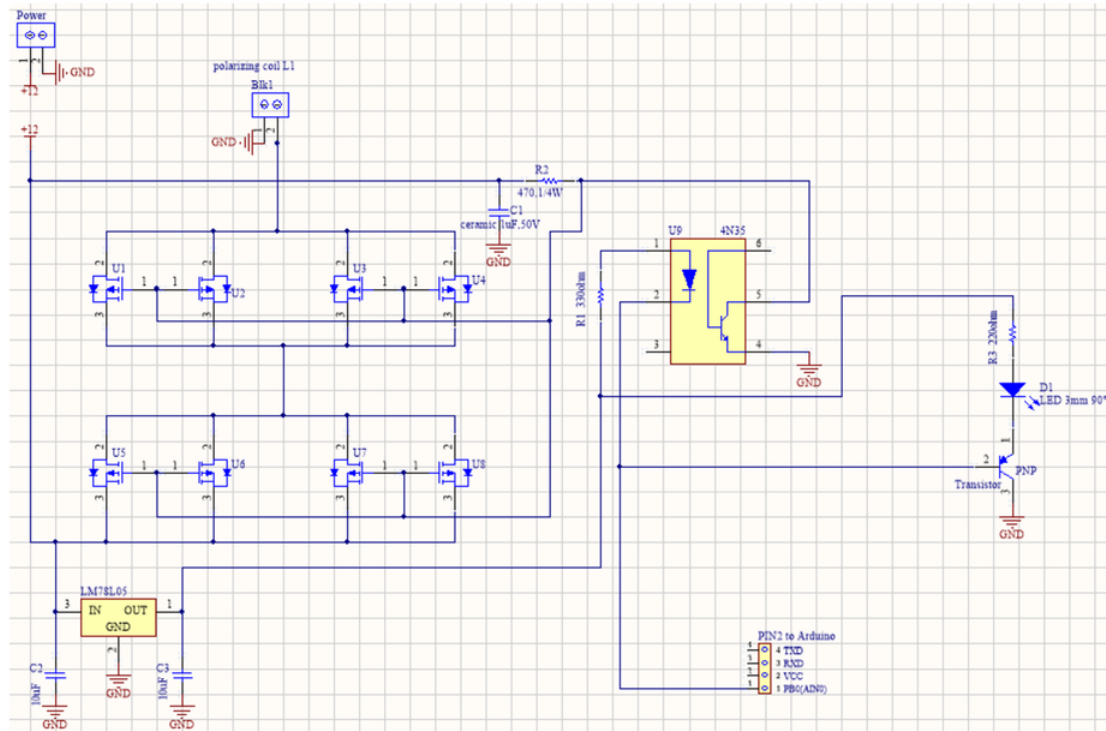


Figure 3.3: Schematic of the pulse controller

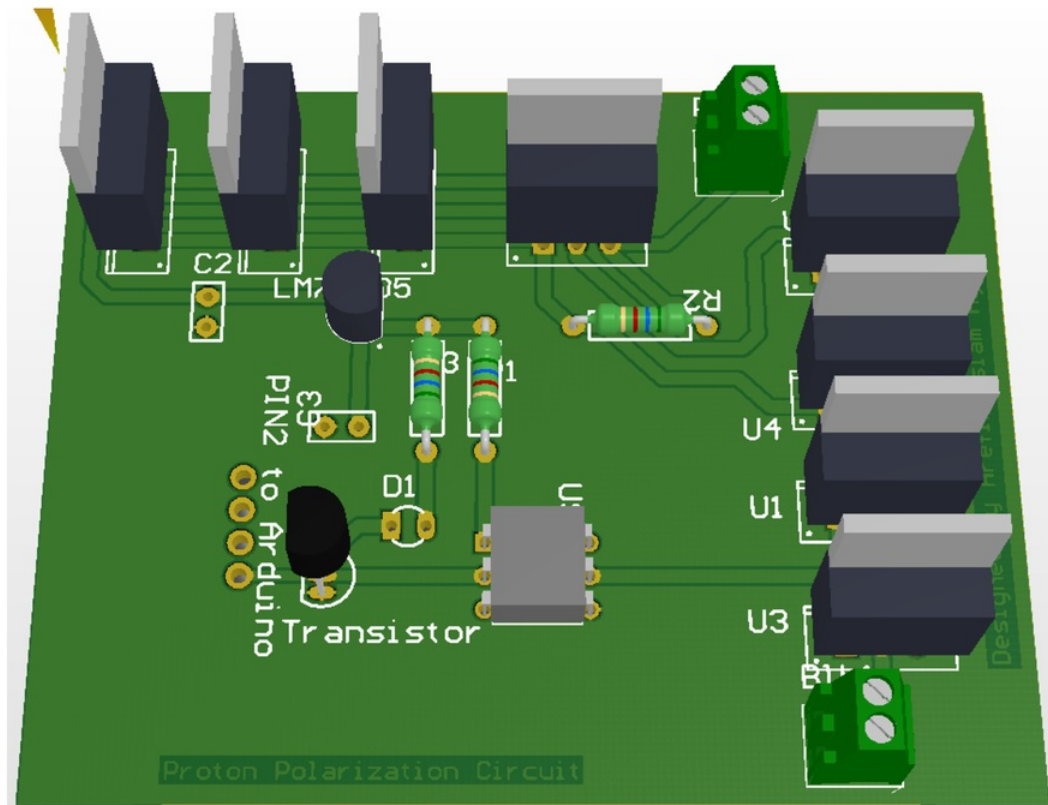


Figure 3.4: PCB design of the pulse controller

age of 150 Volts. Therefore rearranging the MOSFETs together as shown in the schematic will result in an effective ON-resistance of 0.15 OHMS and a breakdown voltage of 300 Volts. Other MOSFETs can also be used in the design as long as the parameters are similar to IRF6215. As we can see in the circuit that a +12 volt power is directly connected to the source terminals of the first parallel combination of the IRF6215s and the polarization coil is connected directly to the drain terminals of the second parallel combination of IRF6215's. The gate voltage level on all of the eight mosfet is controlled by using an Arduino. To prevent any harm to the Arduino due to large voltage induced during switching the gate voltage is controlled via a 4N35 optocoupler. Opto-isolators prevent high voltages from affecting the Arduino by transferring electrical signals between two isolated circuits by using light. As the output of the pin PB0 on the arduino gets high the transistor on the output side of the opto-isolator is turned off. This makes the gate voltage of the IRF6215's to be approximately +12 Volts so that the source to gate voltage is almost zero which keeps the devices to be turned off. But when the pin P0 gets low the transistor of the 4N35 Opto-coupler is turned on, which makes the gate voltage of the IRF6215's to be about 1 Volt. The gate to source voltage then becomes approximately to be -11 Volts. And because we are using P-channel Mosfet, the IRF6215's turns on at this negative voltage thus allowing the current to pass through the coil.

3.3 Sensor Coil

After the sample has been polarized by using the polarization coil we require sensor coils to acquire the proton precession signal from the sample and then to feed that signal to the amplifier as much as possible.

3.3.1 Sensor Coil Requirements

The sensor coil sits inside the 'Polarization Coil' and the sample sits inside the sensor coil. Therefore for easy access and setup we used solenoid geometry for the sensor coils which allows us to do quick replacement of the sample. Another issue that needs to be considered while designing the sensor coil is the noise that are in the environment. Our world has abundance of man made magnetic fields which are unwanted and the sensor coil will pick up some of this unwanted signals. Thus to defend this issue we have used two identical sensor coils instead of one. The two sensor coils are wound in opposite direction corresponding to each other and then joined as a series connection. The two sensor coils are then mounted parallel to each other inside the polarization coil. Mounting the sensor coils this way helps the external magnetic field noise common to both coils to be canceled out [3]. This setup of the sensor coils helps the sample from the sample coil to be detected with very minimal noise. This entails that the sample needs to be placed in either of the sensor coils because if there are samples in both the sensor coils then there will be a signal produced in each coil and those two signals will then exactly cancel each other resulting in no precessing signal at all.

Another important aspect of the design is that the device is designed to operate using the Earth's magnetic field. Therefore the device needs to be operated in a place where there is no to a minimal ferromagnetic or metallic objects nearby to have a minimal disturbance of the field. As any non-uniformity in the field will cause the output signal to be lost. We also have to consider that large metallic objects that are not ferromagnetic such as aluminum or copper should also be kept away from the coils [3]. The reason for this is because when the current in the polarization coil is turned off, those non ferromagnetic materials can induce eddy currents [9] which then degenerates the magnetic field around the sample coil.

3.3.2 Sensor coil specification

- 22AWG enameled copper magnet wire, diameter=0.6mm
- inner diameter=36mm
- coil length=9mm
- number of layers= 4
- turns per layer = 140, total turns=560
- approximate inductance = 3.1mH

3.3.3 Choosing the correct wire and Construction of the Sensor coils

Choosing the right wire to construct the sensor coil is an important part of the design process. In one side we want thin wires because the more turns we have the more stronger the signal will be and on the other side we want fat wire so that the Johnson noise is low and the quality factor (Q) is high, where Johnson noise is the electronic noise caused by the thermal agitation of electrons in the conductor carrying current [10] and the Q factor is the quality factor which is dimensionless that determines how under-damped an oscillator or a resonator is. It is always better to have a higher Q factor as it represents low energy loss relative to the stored energy of the resonator which means the signal diminishes much more slowly [11]. Thus we chose 22 AWG solid copper enameled magnet wire which fits the above constraints [3].

The next important step is winding the two sensor coils correctly because if wired incorrectly then the ambient noise will not cancel out but amplified. The two coils are wound in opposite directions to each other around an acrylic tube. The tube has a outer diameter of 40mm and an inner diameter of 36mm. The length of the tubes are same as of the polarization coil tube. The same steps as of the polarization coiling process have been followed to complete the coiling of the sensor coils.

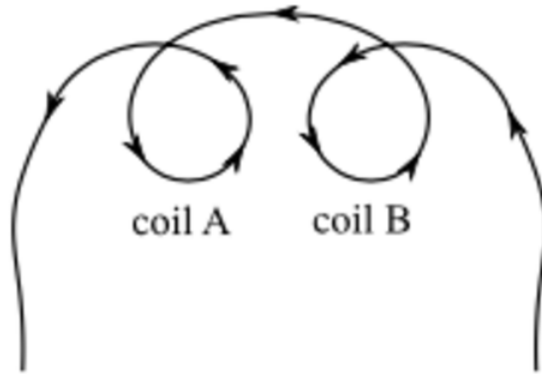


Figure 3.5: Sensor coils wire direction [3]

3.4 Amplifier

The signal that we will be receiving from the sensor coils are very small therefore it is needed to bring the signal to a level where it can be digitized by the Arduino. This role is played by the amplifier. While the amplifier is less complex than the pulse controller but it is more sensitive to how it is constructed [3].

Figure 3.5 shows the amplifier circuit schematic which has been designed in the software 'Circuit Maker' by 'Altium'. The first thing that is noticed that there is a bank of capacitors at the input of the circuit which are used to tune the circuit by using the dip switch. The tuned capacitor value totally depends on some measurements and calculations which is explained in the latter part of the report. The next thing that we notice is the first INA126 instrumentation amplifier. As we can see from the schematic that the output of the first INA126 feeds into an audio transformer. The purpose of the transformer firstly is to prevent the DC voltage from the output of the first INA126 going into the input of the second INA126 because this will just amplify the DC voltage and we do not want that. The second purpose of the transformer is to filter the signal. As our Earth's field signal will be around 2.3KHz [3], the audio transformer works similar to a bandpass filter that attenuates more higher frequencies and much lower frequencies than 2.3KHz. After the audio transformer is the second INA126. The purpose of this is to provide more gain of the attenuated signal. The gain of the first INA126 with its 430hm resistor is around $5+80k/43=1865$. Similarly the second INA126 has a gain of 1865, therefore the total combined gain is about 1865^2 which is around 3478225. After that the output of the 2nd INA126 is passed through an Op177G op-amp. This Op-amp circuit works as a limiter-buffer in here. It basically limits the output of the amplifier to be between +10 volts and -10 volts.

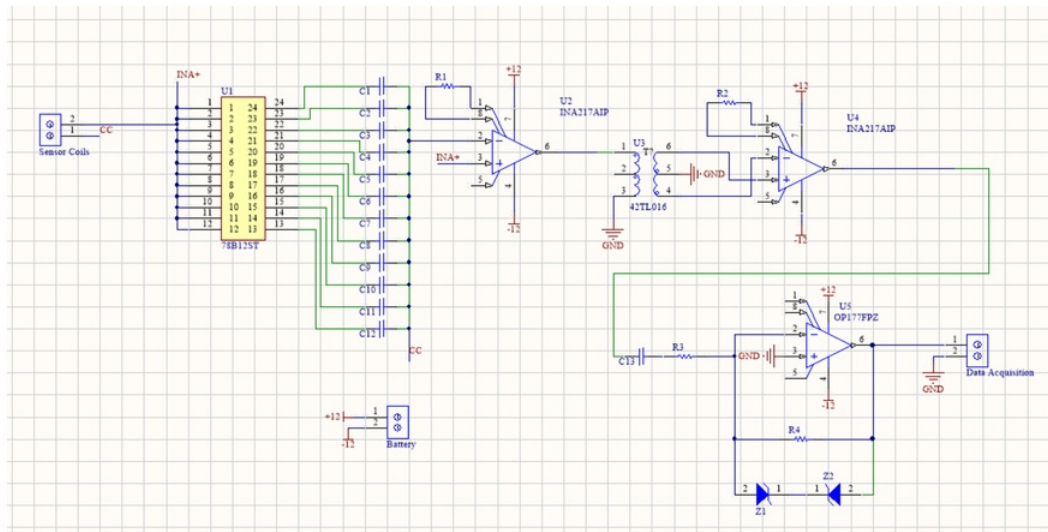


Figure 3.6: Amplifier Circuit Schematic

3.4.1 Advantage of Differential Amplifier

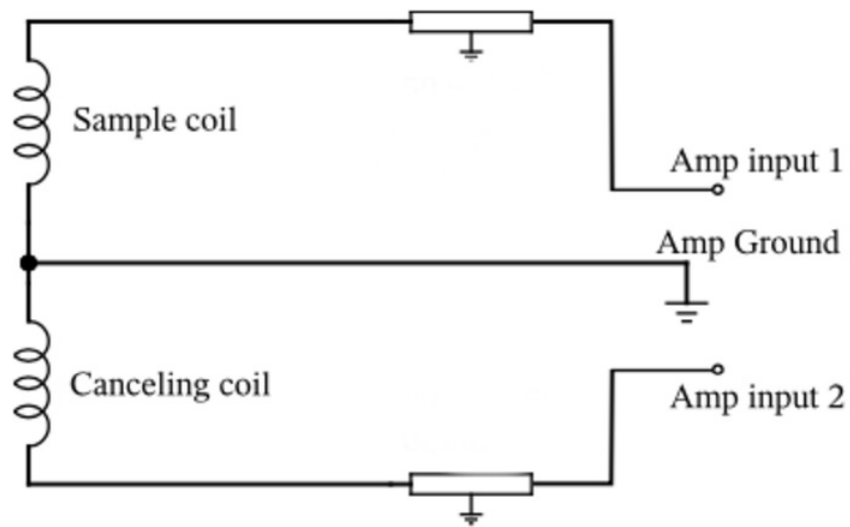


Figure 3.7: Sensor inputs to the Amplifier

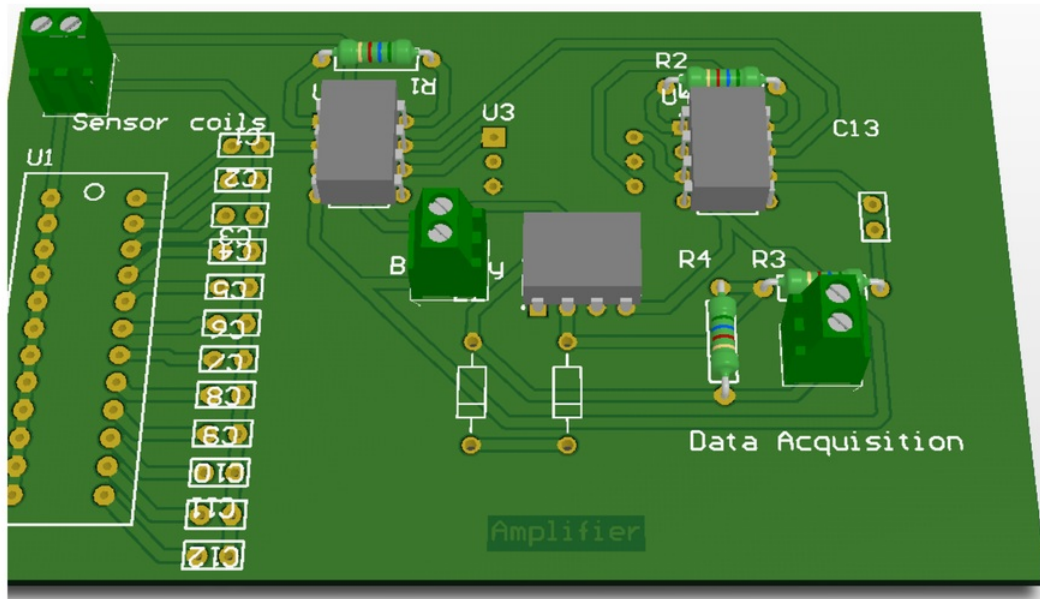


Figure 3.8: Amplifier PCB

Figure 3.6 shows the two inputs to the amplifier from the sensors. The ground of the amplifier is connected to a point between the connections of the sample and the canceling coils. The other two opposite ends of the coils are connected to the inputs of the amplifier. As the sample will be in either of the sensor coils and the two coils will be identical otherwise therefore the two inputs will just differ in the signal that we want. This differential amplifier will amplify the difference between the two sensor inputs which is the signal we want.

3.4.2 Providing power to the Amplifier

Another prevention that we must take to get our few microvolts of precessing signal to get swamped out with noise is to power the amplifier with a clean and a very stable power. This is because as we can see in the amplifier schematic in figure 3.5 that the circuit requires +12Volts and -12Volts. We can power the circuit by using commercial power supplies but that will not be a feasible option as those power supplies derive the DC supply by converting the AC sources which are too noisy. We can control this noise by using regulators and large capacitors which is called bypassing. But another easy way is to use batteries as they are a very clean source of power. In our design we used 6Volts lantern batteries. Two pair this batteries, each connected in series can provide +12Volts and -12Volts.

3.4.3 Tuning to the Correct Capacitor Value

Placing capacitors in series with the sensor coils at the input before the signal reaches the instrumentation amplifier is an efficient way to boost the signal. This creates an oscillator and its resonant frequency is described by the formula given in 3.2.

$$f = \frac{1}{2\pi\sqrt{LC}} \quad (3.2)$$

Here 'f' is the frequency in Hertz, L is the inductances of the two coil in Henrys and C is the tuned capacitor value in Farads. To get a maximum gain it is required to choose a correct capacitor value so that the oscillator's resonant frequency becomes equal to the Earth's field proton precession frequency. We get the correct capacitor value by using the above formula in 3.2. At first we calculate the inductance of our sensor coils in this website '<http://electronbunker.ca/eb/InductanceCalcML.html>'. It requires a bunch of parameters to get the correct inductance of the coil. Parameters required are

- number of turns per Layer - N
- number of layers - N(L)
- coil inside diameter - ID
- wire diameter - d
- Wire Diameter including insulation - di

By putting the above parameters in the website we calculated our coil inductances to be approximately (2*3.1 mH). And now to use the formula in 3.2 we require the precession frequency of the Earth's magnetic field. To get this value we again use the website of 'National Centers for Environmental Information'. We put our desired location in the website and then it returns us the local magnetic field strength value which is '57023.5 nT'. After that we use this magnetic field strength value in this website [12] which returns us the precession frequency which is 2.43 KHz. Then we put all these parameter values in the formula 3.2 to get or desired capacitor value.

Another important fact to keep in mind is that, the Earth's field can change significantly at various locations which means the capacitor value also varies at different location. For this reason, instead of putting one specific capacitor value in our circuit board there is a bank of capacitors. Also at the input of the amplifier is a 12 position DIP switch. The DIP switch number and the corresponding capacitor value is shown in the table below.

DIP switch Number	Capacitor Value(uF)
1	0.0010
2	0.0022
3	0.0039
4	0.0056
5	0.010
6	0.022
7	0.039
8	0.056
9	0.10
10	0.22
11	0.39
12	0.56

It is possible to choose the correct combination of capacitor that is close to the Earth's field proton precession frequency at the current position. We get the required capacitor value by solving C in the above frequency equation. As we already know all the other parameters in the equation we calculated our required capacitor value to be $0.684\mu\text{F}$. And since all the capacitors in our amplifier circuit are in parallel to each other, then according to elementary circuit theory we know that if capacitors are in parallel, therefore the total capacitance is just the sum of all the capacitors. As shown in figure 3.7 the total capacitance is therefore given by the following formula. Therefore to choose the capacitor value equal to the estimated precession frequency of the Earth which is $0.684\mu\text{F}$, we choose dip switches 2, 6, 9 and 12 that will give us total capacitance of

$$C_{\text{total}} = 0.56 + 0.10 + 0.022 + 0.0022 = 0.6842\mu\text{F}$$

$$C_{\text{total}} = C_1 + C_2 + \dots C_n \quad (3.3)$$

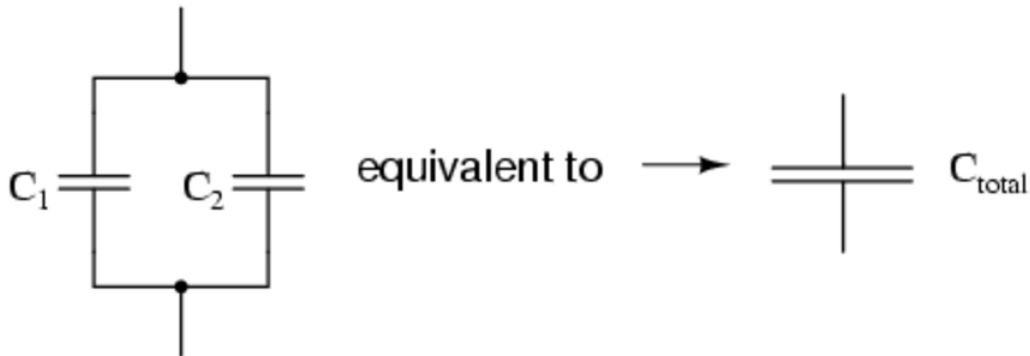


Figure 3.9: Capacitance in Parallel

3.5 Data Acquisition Process

3.5.1 Sampling Rate and resolution

Selecting the sampling rate is a very important part of the data acquisition process. The sampling rate is required to be at least twice the highest frequency component present in the signal to eliminate aliasing, therefore as we know that the Earth's magnetic field frequency is around 2.4 KHz we have to take the sampling frequency as 5KHz that is 10 Kilo samples per second. As we have discussed above in the previous parts, the signal that we will be receiving can be represented in many ways but in our case we are using the analog input pin of an arduino to get the signal. And as the arduino has 10 bit resolution, then the signal that we will be receiving will have a range between 0-1023 units. Also the signal that we will be receiving will be limited to -10V to 10V by the OP-amp which acts as a buffer, thus we scaled down our values to volts by dividing 10/1024 which gives us 0.00976562 v per unit of 1024.

In the Earth's magnetic field, we will always get our precession frequencies within the range of 1.5 KHz to 2.4 KHz. Thus we took the sampling frequency to be 5 KHz.

The whole device is controlled by an arduino. The arduino code that is used to run the design has been shown below.

The way the code works is that, the device always starts in the off mode. The arduino is high when it is turned on and since we are using the P-Channel MOSFET high in arduino means +ve voltage in the gate which in makes the MOSFET's to be turned off. It remains off like this for 10 seconds and then the arduino digital pin goes to low from high which drops the gate voltage of the P-Channel MOSFET. Dropping the gate voltage of the MOSFETs turns on the device and lets the current pass through the coil. It then takes 6 seconds before the MOSFETs are turned off again by making the arduino pin high. After that there is a waiting period of 100 Milli seconds before the arduino analog pin starts taking data. The data is then imported to MATLAB where further processing and filtering is done to remove noise from the signal. The final results are shown below in the results section.

```
int sensor = 1;
int coil = 13;
int val = 0;
int count = 0;
double volt=0.0;

void setup() {
  Serial.begin(1000000);
  pinMode(coil, OUTPUT);
  pinMode(A1, INPUT);

  digitalWrite(coil, HIGH);
  delay(10000); //off coil for 10 sec
  digitalWrite(coil, LOW); // on coil for 6 sec
  delay(6000);
  digitalWrite(coil, HIGH); //Turn off Coil for 100ms before reading the data from sensor coils
  delay(100);
}

void loop() {

  if (count <10000)
  {
    delayMicroseconds(100); //sample interval
    val = analogRead(A1); //store sensor value (0-1023) //takes 100ms to read data
    count++;

    volt = val*0.00976562;
    Serial.print(volt); //takes 100ms to print data thus interval between each sample 200ms
    Serial.println();
  }
}
```

Figure 3.10: Arduino Code

Chapter 4

Results and Discussions

4.1 Results

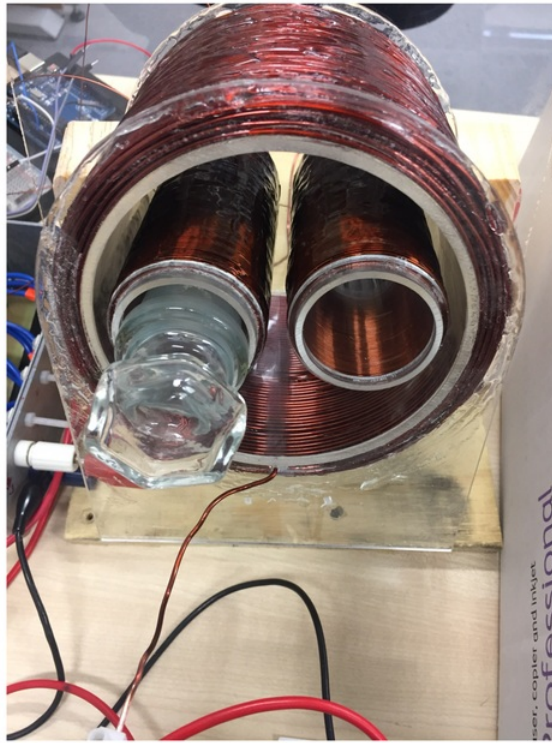


Figure 4.1: Polarization coil housing two sensor coils

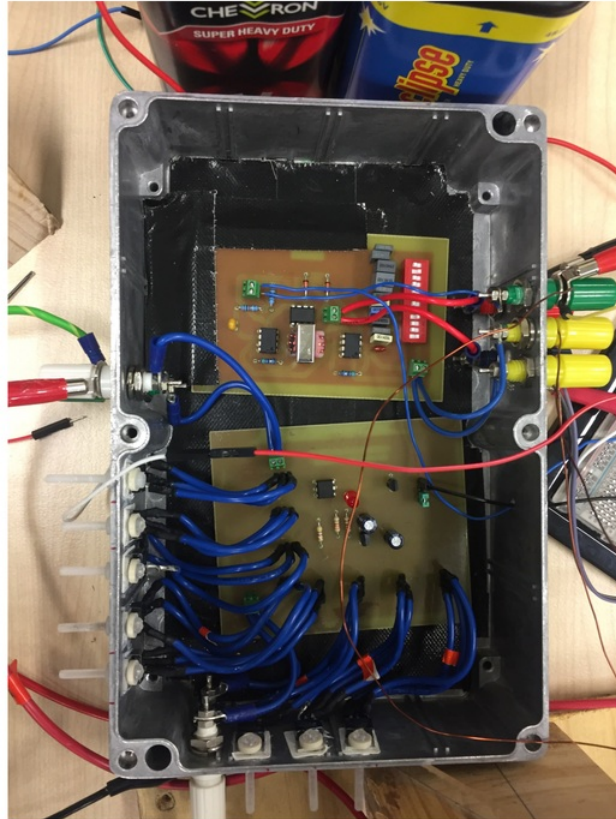


Figure 4.2: Amplifier and the Polarization circuit

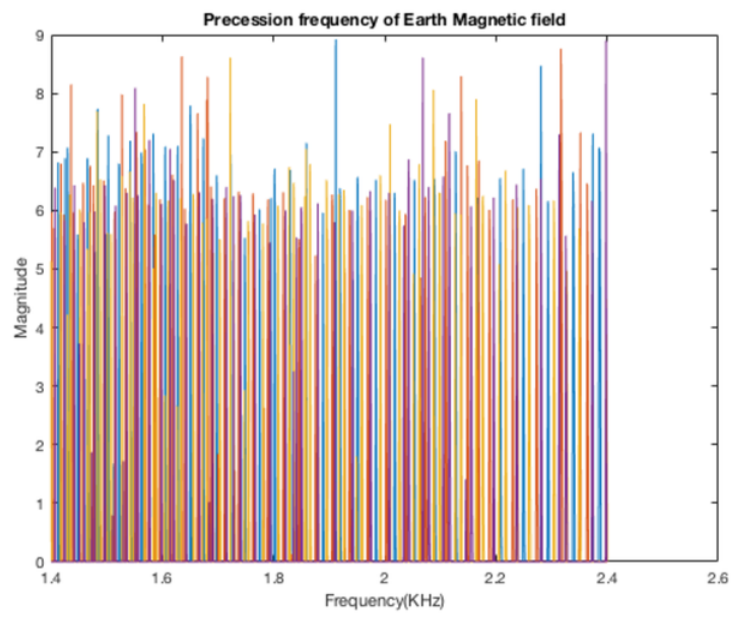


Figure 4.3: Raw data with noise

4.2 Discussions

Figure 4.1 is the picture of the coil that has been manually wound as a part of the design. The bigger coil is the polarization coil which houses the two sensor coils. One of the sensor coil (left) is where the hydrogen sample is placed and the other one (right) is kept free as it will be used to cancel out the environmental noise.

Figure 4.2 is the enclosure that houses the two PCB, polarization circuit and the amplifier circuit and also shows the total setup. As we have discussed earlier that the MOSFETs will get hot, thus for cooling down purposes the MOSFETs are mounted on the enclosure side walls.

After the device is turned on, the polarization process takes place and then comes the signal acquisition process. Figure 4.5 shows a similar overview of the process that takes place.

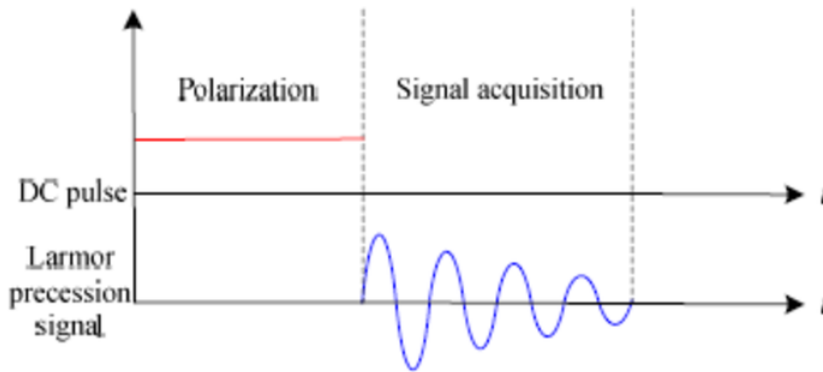


Figure 4.4: Running sequence

4.2.1 Noisy Signal

Figure 4.2 is the received data signal received from Arduino analog pin. The data that we received is very noisy which was beyond our expectation. It did not show any precession signal from the proton. There are couple of possible reasons which might be causing the problem.

The first problem that was addressed is, the signal that we are receiving from the op amp OP177G in our amplifier limits the signal which has a range of -10 Volts to 10 Volts and the arduino model that we used have the ability to detect analog input within the range of 0V - 5V which clearly shows that most of the signals are getting saturated which is the reason we end up getting no precession signal at all. Another reason could be is that, the lab we did our tests on had object containing ferromagnetic materials and many power lines which might be the reason of electromagnetic interference that caused the signal to be swamped away.

To overcome the first problem, that is to produce a signal that the arduino can detect is to include a summing op-amp circuit in the amplifier PCB. The circuit schematic for this specific purpose has been shown in figure 4.5.

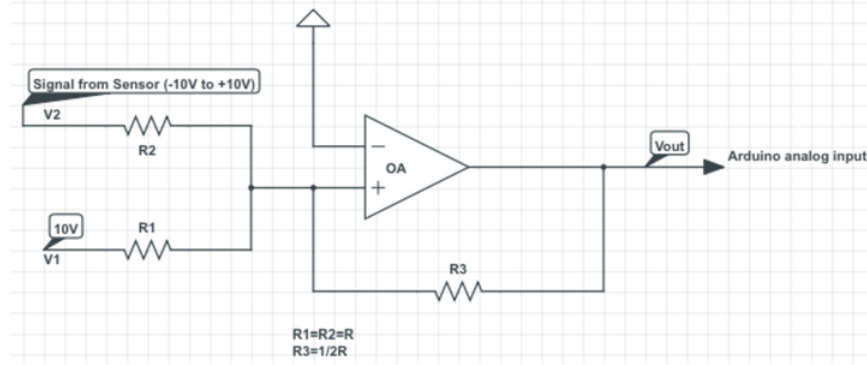


Figure 4.5: Amplifier summing circuit

The figure shows that, if we already have a signal V_1 in the range of (-10V to 10V) from the sensor and then we add another 10 volts DC supply and arrange this in the way it is shown in figure 4.5 then the V_{out} will be according to the equation 4.1 .

$$V_{out} = \frac{R_3}{R_1} V_1 + \frac{R_3}{R_2} V_2, \text{ where } R_1 = R_2 = R \quad (4.1)$$

If we update the circuit like this then the original signal will be just shifted like the picture shown in figure 4.6. Thus, the -10V will shift to 0V and the +10Volts will shift to 20V. Notice that, the output will be 20V only when $R_1 = R_2 = R_3$ and we do not want that. This is because we already mentioned that arduino will be able to detect signals from 0V to 5V only, thus we need to adjust the resistor values so that the gain is always half of input signal. The equation of the required resistor value is shown in equation 4.2.

$$R_1 = R_2 = R \quad (4.2)$$

$$R_3 = \frac{1}{2} R \quad (4.3)$$

Therefore we have to choose the resistor values so that it satisfies the equation 4.2 and 4.3 to get the range of V_{out} between 0V to 5V which is detectable by the arduino.

Again to overcome the second problem, that is to avoid interference by the ferromagnetic objects, the tests are required to run in outdoor environment conditions. For this we require longer power cable to power the coils from the source.

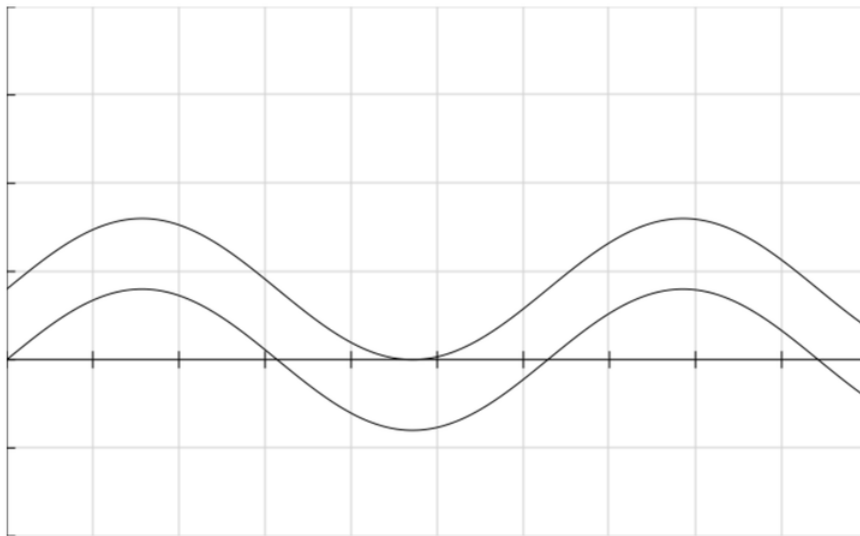


Figure 4.6: Shifting of the signal

Chapter 5

Conclusions and Future Work

5.1 Conclusions

This thesis mainly focused in prototyping a proton precession magnetometer (PPM) which can lead us to explore the possibilities of cheaper MRI technology. Prototyping the magnetometer in order to detect the Earth's magnetic field frequency was the project goal of this thesis, however in longer term the research can be further extended for other industrial and biomedical applications.

The whole process in prototyping this PPM has been explained throughout the thesis. The results above indicates that the designed PPM is not yet completely ready to measure the Earth's magnetic field due to some limitations and issues that arose during the prototyping process. The first limitation was that Arduino analog input's voltage range 0V to 5V which was not compatible to our prototype as our signal has range from -10V to 10V. For this reason the signals were always in the saturation stage which ends up with no precession signal. Possible solution to the problem have been discussed. Solution to the second problem was also addressed which is to conduct further experiments outdoors, where there is minimal ferromagnetic objects so that there is no electromagnetic interference.

5.1.1 Future Work

It is recommended to use longer wires so that the coils can be kept further apart from power lines and ferromagnetic objects. Using coax cable for the sensor inputs is also a good option as this will minimize the risk of the tiny signal of the proton precession to be lost before reaching the amplifier.

It is recommended to design the summing circuit in a PCB board however for testing purposes a bread board can be used. It is necessary to use a 150Watt power supply to power the polarization coil. This will ensure that the coil produces much larger magnetic field which will confirm that all almost all the protons in the sample are polarized.

Appendix A

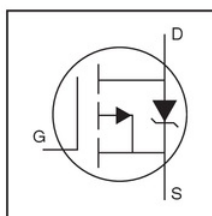
Data sheets of components used in the circuit

A.1 Datasheet of MOSFET used for the polarization circuit

IRF6215PbF

HEXFET® Power MOSFET

- Advanced Process Technology
- Dynamic dv/dt Rating
- 175°C Operating Temperature
- Fast Switching
- P-Channel
- Fully Avalanche Rated
- Lead-Free

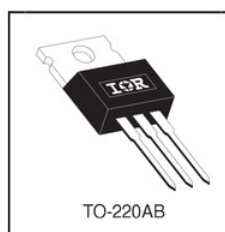


$V_{DS} = -150V$
 $R_{DS(on)} = 0.29\Omega$
 $I_D = -13A$

Description

Fifth Generation HEXFETs from International Rectifier utilize advanced processing techniques to achieve extremely low on-resistance per silicon area. This benefit, combined with the fast switching speed and ruggedized device design that HEXFET Power MOSFETs are well known for, provides the designer with an extremely efficient and reliable device for use in a wide variety of applications.

The TO-220 package is universally preferred for all commercial-industrial applications at power dissipation levels to approximately 50 watts. The low thermal resistance and low package cost of the TO-220 contribute to its wide acceptance throughout the industry.



Absolute Maximum Ratings

	Parameter	Max.	Units
I_D @ $T_C = 25^\circ C$	Continuous Drain Current, V_{GS} @ -10V	-13	A
I_D @ $T_C = 100^\circ C$	Continuous Drain Current, V_{GS} @ -10V	-9.0	
I_{DM}	Pulsed Drain Current ①	-44	
P_D @ $T_C = 25^\circ C$	Power Dissipation	110	W
	Linear Derating Factor	0.71	W/°C
V_{GS}	Gate-to-Source Voltage	± 20	V
E_{AS}	Single Pulse Avalanche Energy ②	310	mJ
I_{AR}	Avalanche Current ③	-6.6	A
E_{AR}	Repetitive Avalanche Energy ④	11	mJ
dv/dt	Peak Diode Recovery dv/dt ⑤	-5.0	V/ns
T_J	Operating Junction and	-55 to + 175	°C
T_{STG}	Storage Temperature Range		
	Soldering Temperature, for 10 seconds	300 (1.6mm from case)	
	Mounting torque, 6-32 or M3 screw	10 lbf•in (1.1N•m)	

Thermal Resistance

	Parameter	Typ.	Max.	Units
$R_{\theta JC}$	Junction-to-Case	—	1.4	°C/W
$R_{\theta CS}$	Case-to-Sink, Flat, Greased Surface	0.50	—	
$R_{\theta JA}$	Junction-to-Ambient	—	62	

IRF6215PbF

International
IR Rectifier

Electrical Characteristics @ $T_J = 25^\circ\text{C}$ (unless otherwise specified)

	Parameter	Min.	Typ.	Max.	Units	Conditions
$V_{(BR)DSS}$	Drain-to-Source Breakdown Voltage	-150	—	—	V	$V_{GS} = 0V, I_D = 250\mu A$
$\Delta V_{(BR)DSS}/\Delta T_J$	Breakdown Voltage Temp. Coefficient	—	-0.20	—	V/ $^\circ\text{C}$	Reference to $25^\circ\text{C}, I_D = 1mA$
$R_{DS(on)}$	Static Drain-to-Source On-Resistance	—	—	0.29	Ω	$V_{GS} = -10V, I_D = -6.6A$ ①, $T_J = 25^\circ\text{C}$
		—	—	0.58		$V_{GS} = -10V, I_D = -6.6A$ ①, $T_J = 150^\circ\text{C}$
$V_{GS(th)}$	Gate Threshold Voltage	-2.0	—	-4.0	V	$V_{DS} = V_{GS}, I_D = -250\mu A$
g_{fs}	Forward Transconductance	3.6	—	—	S	$V_{DS} = -50V, I_D = -6.6A$
I_{DSS}	Drain-to-Source Leakage Current	—	—	-25	μA	$V_{DS} = -150V, V_{GS} = 0V$
		—	—	-250		$V_{DS} = -120V, V_{GS} = 0V, T_J = 150^\circ\text{C}$
I_{GSS}	Gate-to-Source Forward Leakage	—	—	100	nA	$V_{GS} = 20V$
	Gate-to-Source Reverse Leakage	—	—	-100		$V_{GS} = -20V$
Q_g	Total Gate Charge	—	—	66		$I_D = -6.6A$
Q_{gs}	Gate-to-Source Charge	—	—	8.1	nC	$V_{DS} = -120V$
Q_{gd}	Gate-to-Drain ("Miller") Charge	—	—	35		$V_{GS} = -10V$, See Fig. 6 and 13 ②
$t_{d(on)}$	Turn-On Delay Time	—	14	—	ns	$V_{DD} = -75V$ $I_D = -6.6A$ $R_G = 6.8\Omega$ $R_D = 12\Omega$, See Fig. 10
t_r	Rise Time	—	36	—		
$t_{d(off)}$	Turn-Off Delay Time	—	53	—		
t_f	Fall Time	—	37	—		
L_D	Internal Drain Inductance	—	4.5	—	nH	Between lead, 6mm (0.25in.) from package and center of die contact
L_S	Internal Source Inductance	—	7.5	—		
C_{iss}	Input Capacitance	—	860	—	pF	$V_{GS} = 0V$ $V_{DS} = -25V$ $f = 1.0MHz$, See Fig. 5
C_{oss}	Output Capacitance	—	220	—		
C_{rss}	Reverse Transfer Capacitance	—	130	—		

Source-Drain Ratings and Characteristics

	Parameter	Min.	Typ.	Max.	Units	Conditions
I_S	Continuous Source Current (Body Diode)	—	—	-13	A	MOSFET symbol showing the integral reverse p-n junction diode.
I_{SM}	Pulsed Source Current (Body Diode) ③	—	—	-44		
V_{SD}	Diode Forward Voltage	—	—	-1.6	V	$T_J = 25^\circ\text{C}, I_S = -6.6A, V_{GS} = 0V$ ④
t_{rr}	Reverse Recovery Time	—	160	240	ns	$T_J = 25^\circ\text{C}, I_F = -6.6A$
Q_{rr}	Reverse Recovery Charge	—	1.2	1.7	μC	$di/dt = -100A/\mu s$ ④
t_{on}	Forward Turn-On Time	Intrinsic turn-on time is negligible (turn-on is dominated by $L_S + L_D$)				

Notes:

- ① Repetitive rating; pulse width limited by max. junction temperature. (See fig. 11)
- ② Starting $T_J = 25^\circ\text{C}$, $L = 14mH$
 $R_G = 25\Omega$, $I_{AS} = -6.6A$. (See Figure 12)
- ③ $I_{SD} \leq -6.6A$, $di/dt \leq -620A/\mu s$, $V_{DD} \leq V_{(BR)DSS}$,
 $T_J \leq 175^\circ\text{C}$
- ④ Pulse width $\leq 300\mu s$; duty cycle $\leq 2\%$.

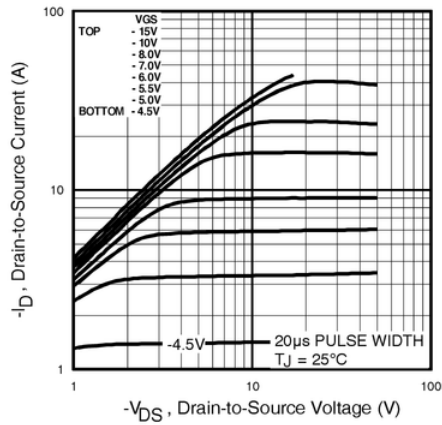


Fig 1. Typical Output Characteristics,

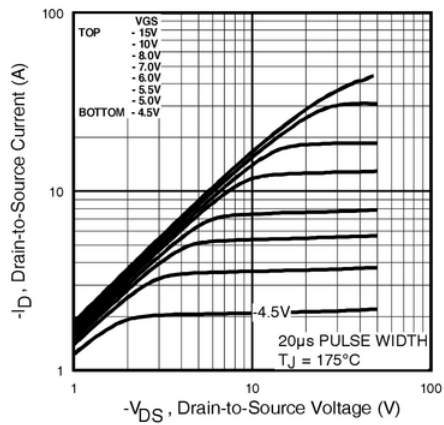


Fig 2. Typical Output Characteristics,

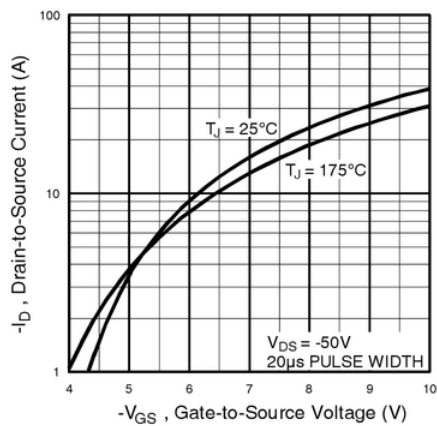


Fig 3. Typical Transfer Characteristics

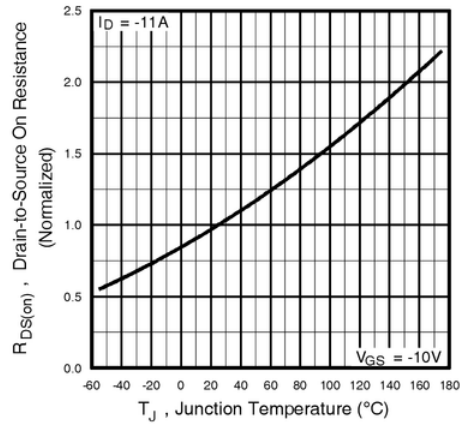
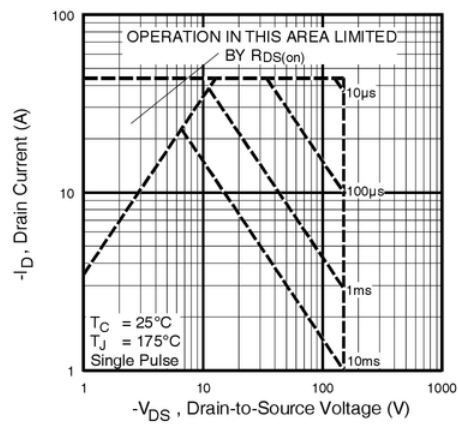
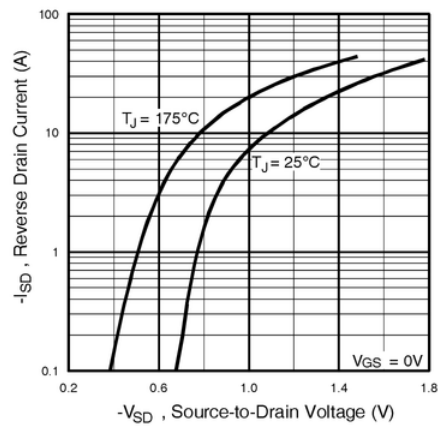
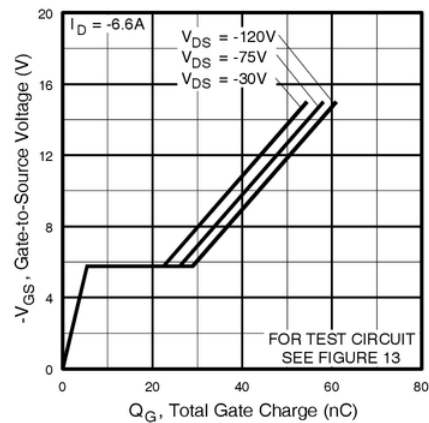
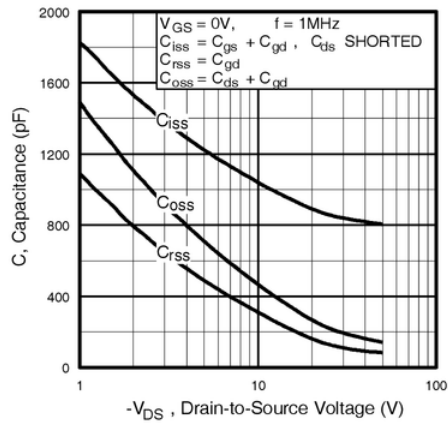


Fig 4. Normalized On-Resistance
Vs. Temperature

IRF6215PbF

International
Rectifier



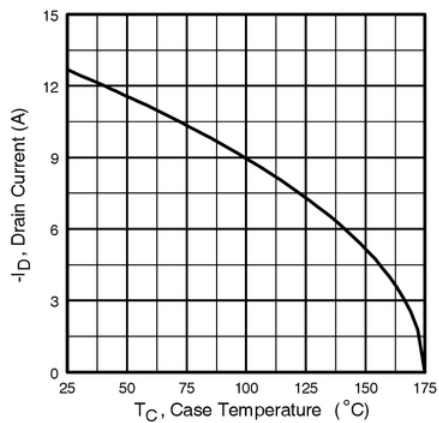


Fig 9. Maximum Drain Current Vs. Case Temperature

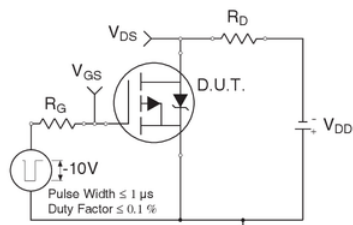


Fig 10a. Switching Time Test Circuit

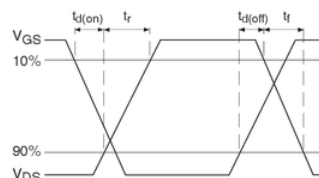


Fig 10b. Switching Time Waveforms

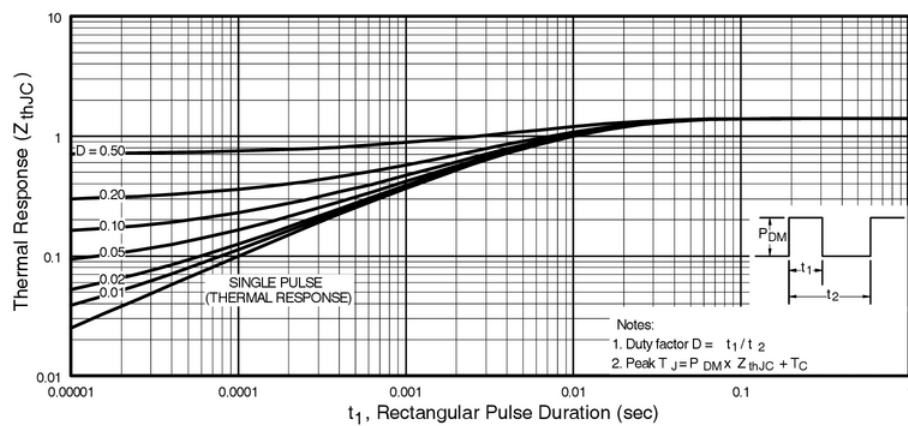


Fig 11. Maximum Effective Transient Thermal Impedance, Junction-to-Case

IRF6215PbF

International
Rectifier

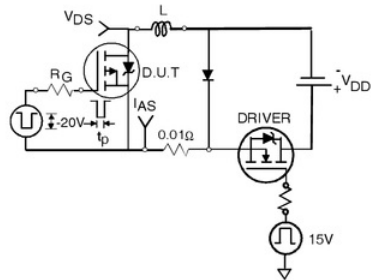


Fig 12a. Unclamped Inductive Test Circuit

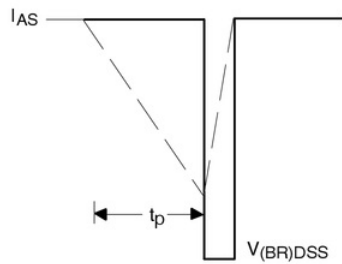


Fig 12b. Unclamped Inductive Waveforms

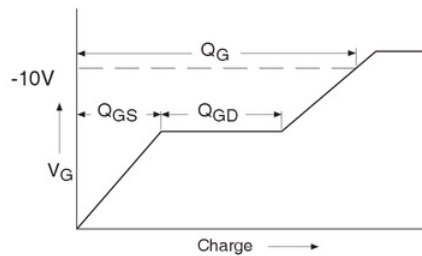


Fig 13a. Basic Gate Charge Waveform

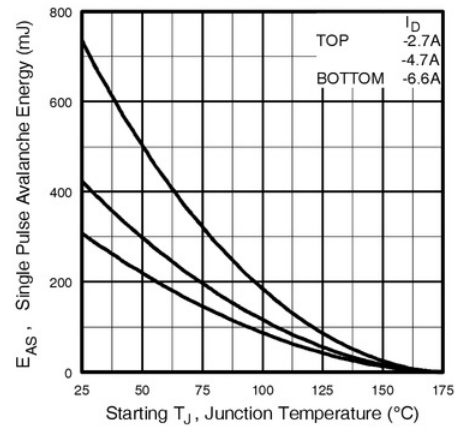


Fig 12c. Maximum Avalanche Energy Vs. Drain Current

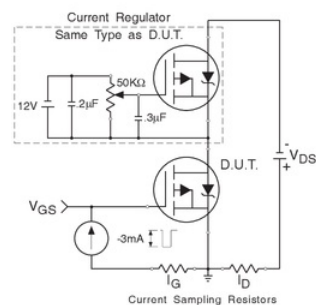
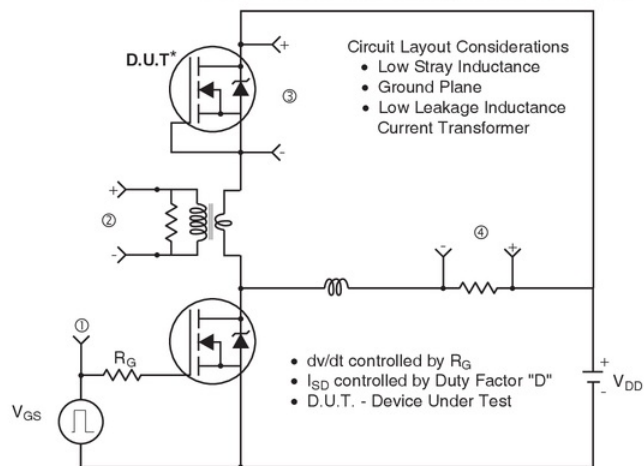
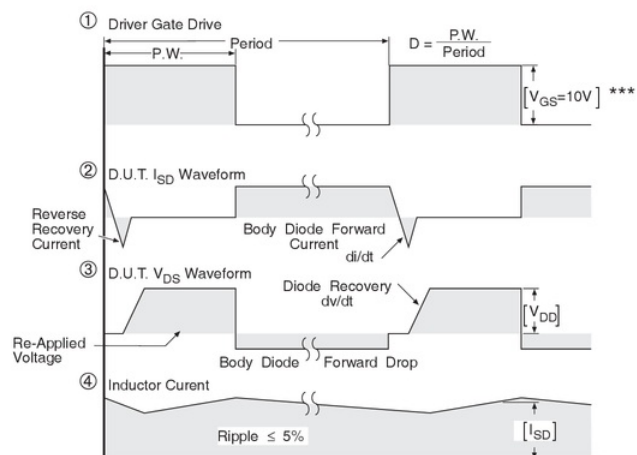


Fig 13b. Gate Charge Test Circuit

Peak Diode Recovery dv/dt Test Circuit



* Reverse Polarity of D.U.T for P-Channel

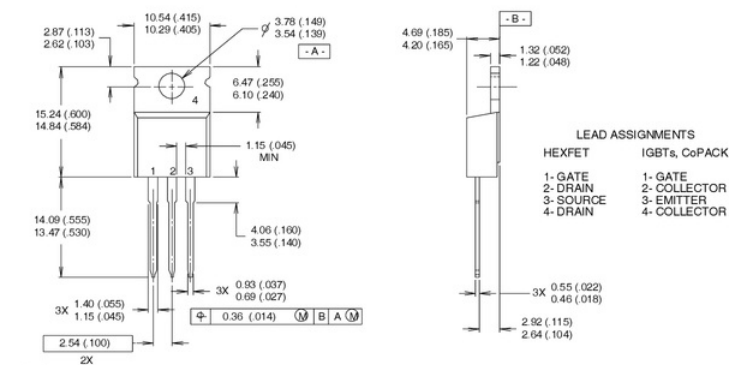


*** $V_{GS} = 5.0V$ for Logic Level and 3V Drive Devices

Fig 14. For P-Channel HEXFETS

International
IOR Rectifier

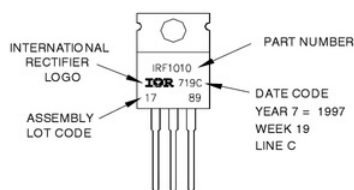
Dimensions are shown in millimeters (inches)



NOTES:

1 DIMENSIONING & TOLERANCING PER ANSI Y14.5M, 1982	3 OUTLINE CONFORMS TO JEDEC OUTLINE TO-220AB.
2 CONTROLLING DIMENSION : INCH	4 HEATSINK & LEAD MEASUREMENTS DO NOT INCLUDE BURRS

EXAMPLE: THIS IS AN IRF1010
LOT CODE 1789
ASSEMBLED ON WW 19, 1997
IN THE ASSEMBLY LINE "C"
Note: "P" in assembly line
position indicates "Lead-Free"



Data and specifications subject to change without notice.

International
IOR Rectifier

IR WORLD HEADQUARTERS: 233 Kansas St., El Segundo, California 90245, USA Tel: (310) 252-7105
TAC Fax: (310) 252-7903
Visit us at www.irf.com for sales contact information. 11/03

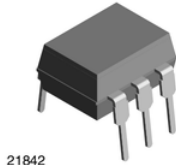
A.2 Optocoupler Data sheet



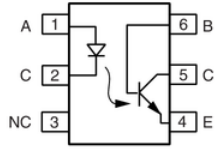
4N35, 4N36, 4N37

Vishay Semiconductors

Optocoupler, Phototransistor Output, with Base Connection



21842



1179004-5

FEATURES

- Isolation test voltage 5000 V_{RMS}
- Interfaces with common logic families
- Input-output coupling capacitance < 0.5 pF
- Industry standard dual-in-line 6 pin package
- Compliant to RoHS directive 2002/95/EC and in accordance to WEEE 2002/96/EC



RoHS
COMPLIANT

APPLICATIONS

- AC mains detection
- Reed relay driving
- Switch mode power supply feedback
- Telephone ring detection
- Logic ground isolation
- Logic coupling with high frequency noise rejection

DESCRIPTION

Each optocoupler consists of gallium arsenide infrared LED and a silicon NPN phototransistor.

AGENCY APPROVALS

- Underwriters laboratory file no. E52744
- BSI: EN 60065:2002, EN 60950:2000
- FIMKO; EN 60065, EN 60335, EN 60950 certificate no. 25156

ORDER INFORMATION

PART	REMARKS
4N35	CTR > 100 %, DIP-6
4N36	CTR > 100 %, DIP-6
4N37	CTR > 100 %, DIP-6

ABSOLUTE MAXIMUM RATINGS ⁽¹⁾

PARAMETER	TEST CONDITION	SYMBOL	VALUE	UNIT
INPUT				
Reverse voltage		V _R	6	V
Forward current		I _F	50	mA
Surge current	t ≤ 10 μs	I _{FSM}	1	A
Power dissipation		P _{diss}	70	mW
OUTPUT				
Collector emitter breakdown voltage		V _{CEO}	70	V
Emitter base breakdown voltage		V _{EBO}	7	V
Collector current		I _C	50	mA
	t ≤ 1 ms	I _C	100	mA
Power dissipation		P _{diss}	70	mW
COUPLER				
Isolation test voltage		V _{ISO}	5000	V _{RMS}
Creepage			≥ 7	mm
Clearance			≥ 7	mm
Isolation thickness between emitter and detector			≥ 0.4	mm

4N35, 4N36, 4N37



Vishay Semiconductors Optocoupler, Phototransistor Output,
with Base Connection

ABSOLUTE MAXIMUM RATINGS ⁽¹⁾				
PARAMETER	TEST CONDITION	SYMBOL	VALUE	UNIT
COUPLER				
Comparative tracking index	DIN IEC 112/VDE 0303, part 1		175	
Isolation resistance	$V_{IO} = 500 \text{ V}$, $T_{amb} = 25 \text{ }^{\circ}\text{C}$	R_{IO}	10^{12}	Ω
	$V_{IO} = 500 \text{ V}$, $T_{amb} = 100 \text{ }^{\circ}\text{C}$	R_{IO}	10^{11}	Ω
Storage temperature		T_{stg}	- 55 to + 150	$^{\circ}\text{C}$
Operating temperature		T_{amb}	- 55 to + 100	$^{\circ}\text{C}$
Junction temperature		T_J	100	$^{\circ}\text{C}$
Soldering temperature ⁽²⁾	max.10 s dip soldering: distance to seating plane $\geq 1.5 \text{ mm}$	T_{sld}	260	$^{\circ}\text{C}$

Notes

⁽¹⁾ $T_{amb} = 25 \text{ }^{\circ}\text{C}$, unless otherwise specified.

Stresses in excess of the absolute maximum ratings can cause permanent damage to the device. Functional operation of the device is not implied at these or any other conditions in excess of those given in the operational sections of this document. Exposure to absolute maximum ratings for extended periods of the time can adversely affect reliability.

⁽²⁾ Refer to wave profile for soldering conditions for through hole devices (DIP).

ELECTRICAL CHARACTERISTICS ⁽¹⁾							
PARAMETER	TEST CONDITION	PART	SYMBOL	MIN.	TYP.	MAX.	UNIT
INPUT							
Junction capacitance	$V_R = 0 \text{ V}$, $f = 1 \text{ MHz}$		C_j		50		pF
Forward voltage ⁽²⁾	$I_F = 10 \text{ mA}$		V_F		1.3	1.5	V
	$I_F = 10 \text{ mA}$, $T_{amb} = - 55 \text{ }^{\circ}\text{C}$		V_F	0.9	1.3	1.7	V
Reverse current ⁽²⁾	$V_R = 6 \text{ V}$		I_R		0.1	10	μA
Capacitance	$V_R = 0 \text{ V}$, $f = 1 \text{ MHz}$		C_O		25		pF
OUTPUT							
Collector emitter breakdown voltage ⁽²⁾	$I_C = 1 \text{ mA}$	4N35	BV_{CEO}	30			V
		4N36	BV_{CEO}	30			V
		4N37	BV_{CEO}	30			V
Emitter collector breakdown voltage ⁽²⁾	$I_E = 100 \text{ }\mu\text{A}$		BV_{ECO}	7			V
OUTPUT							
Collector base breakdown voltage ⁽²⁾	$I_C = 100 \text{ }\mu\text{A}$, $I_B = 1 \text{ }\mu\text{A}$	4N35	BV_{CBO}	70			V
		4N36	BV_{CBO}	70			V
		4N37	BV_{CBO}	70			V
Collector emitter leakage current ⁽²⁾	$V_{CE} = 10 \text{ V}$, $I_F = 0$	4N35	I_{CEO}		5	50	nA
		4N36	I_{CEO}		5	50	nA
	$V_{CE} = 10 \text{ V}$, $I_F = 0$	4N37	I_{CEO}		5	50	nA
		4N35	I_{CEO}			500	μA
	$V_{CE} = 30 \text{ V}$, $I_F = 0$, $T_{amb} = 100 \text{ }^{\circ}\text{C}$	4N36	I_{CEO}			500	μA
		4N37	I_{CEO}			500	μA
			I_{CEO}			500	μA
Collector emitter capacitance	$V_{CE} = 0$		C_{CE}		6		pF
COUPLER							
Resistance, input output ⁽²⁾	$V_{IO} = 500 \text{ V}$		R_{IO}	10^{11}			Ω
Capacitance, input output	$f = 1 \text{ MHz}$		C_{IO}		0.6		pF

Notes

⁽¹⁾ $T_{amb} = 25 \text{ }^{\circ}\text{C}$, unless otherwise specified.

Minimum and maximum values are testing requirements. Typical values are characteristics of the device and are the result of engineering evaluation. Typical values are for information only and are not part of the testing requirements.

⁽²⁾ Indicates JEDEC registered value.



4N35, 4N36, 4N37

Optocoupler, Phototransistor Output, Vishay Semiconductors
with Base Connection

CURRENT TRANSFER RATIO							
PARAMETER	TEST CONDITION	PART	SYMBOL	MIN	TYP.	MAX	UNIT
DC current transfer ratio ⁽¹⁾	$V_{CE} = 10 \text{ V}$, $I_F = 10 \text{ mA}$	4N35	CTR_{DC}	100			%
		4N36	CTR_{DC}	100			%
		4N37	CTR_{DC}	100			%
	$V_{CE} = 10 \text{ V}$, $I_F = 10 \text{ mA}$, $T_A = -55^\circ\text{C}$ to $+100^\circ\text{C}$	4N35	CTR_{DC}	40	50		%
		4N36	CTR_{DC}	40	50		%
		4N37	CTR_{DC}	40	50		%

Note

⁽¹⁾ Indicates JEDEC registered values.

SWITCHING CHARACTERISTICS						
PARAMETER	TEST CONDITION	SYMBOL	MIN.	TYP.	MAX.	UNIT
Switching time ⁽¹⁾	V _{CC} = 10 V, I _C = 2 mA, R _L = 100 Ω	t _{on} , t _{off}		10		μs

Note

⁽¹⁾ Indicates JEDEC registered values.

TYPICAL CHARACTERISTICS

$T_{amb} = 25^\circ\text{C}$, unless otherwise specified

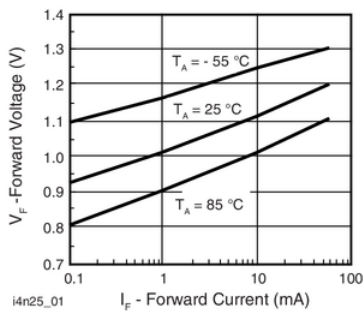


Fig. 1 - Forward Voltage vs. Forward Current

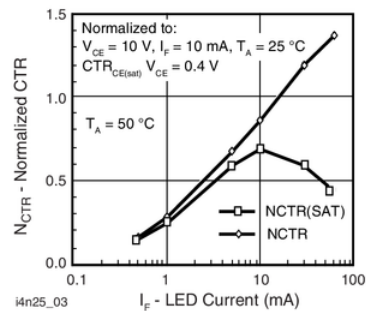


Fig. 3 - Normalized Non-Saturated and Saturated CTR vs. LED Current

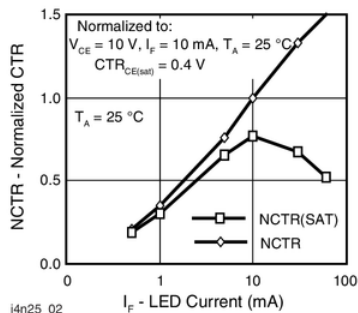


Fig. 2 - Normalized Non-Saturated and Saturated CTR vs. LED Current

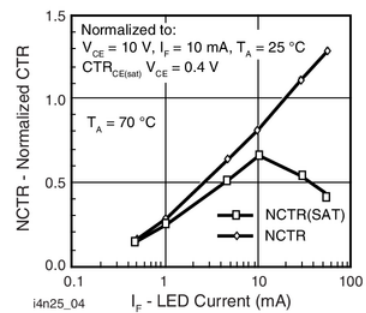


Fig. 4 - Normalized Non-Saturated and Saturated CTR vs. LED Current

4N35, 4N36, 4N37

Vishay Semiconductors Optocoupler, Phototransistor Output,
with Base Connection

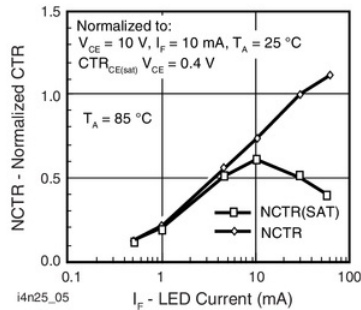


Fig. 5 - Normalized Non-Saturated and Saturated CTR vs. LED Current

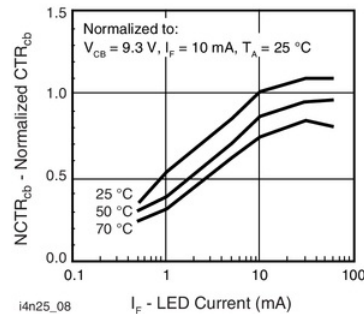


Fig. 8 - Normalized CTR_{cb} vs. LED Current and Temperature

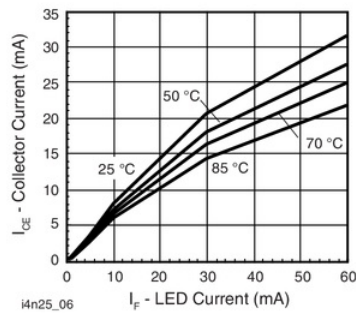


Fig. 6 - Collector Emitter Current vs. Temperature and LED Current

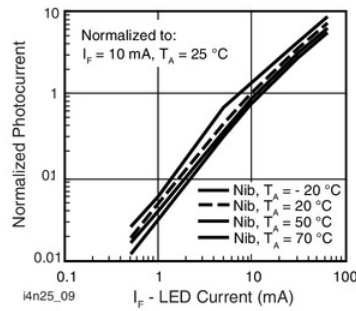


Fig. 9 - Normalized Photocurrent vs. I_F and Temperature

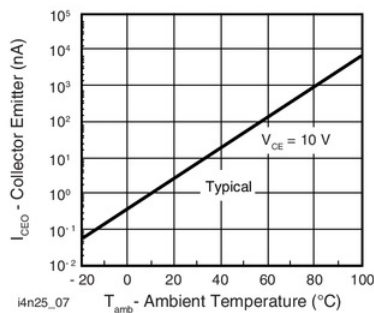


Fig. 7 - Collector Emitter Leakage Current vs. Temperature

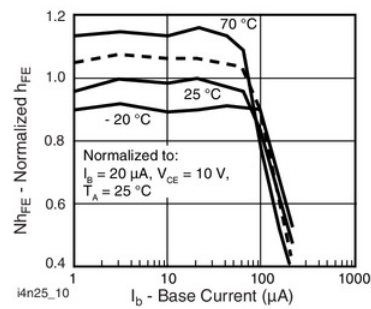


Fig. 10 - Normalized Non-Saturated h_{FE} vs. Base Current and Temperature



4N35, 4N36, 4N37

Optocoupler, Phototransistor Output, Vishay Semiconductors
with Base Connection

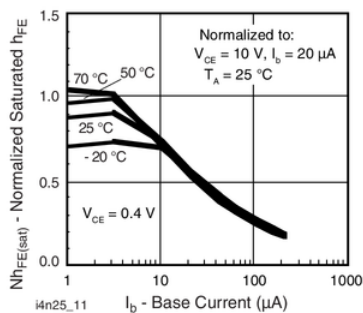


Fig. 11 - Normalized h_{FE} vs. Base Current and Temperature

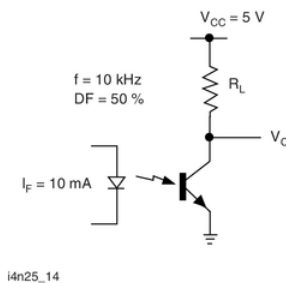


Fig. 14 - Switching Schematic

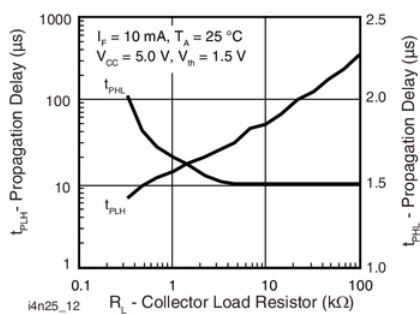


Fig. 12 - Propagation Delay vs. Collector Load Resistor

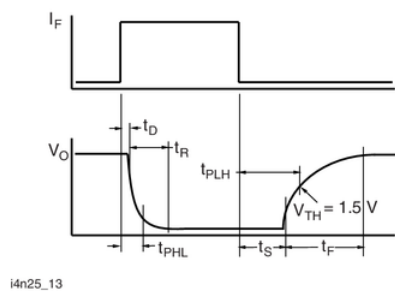


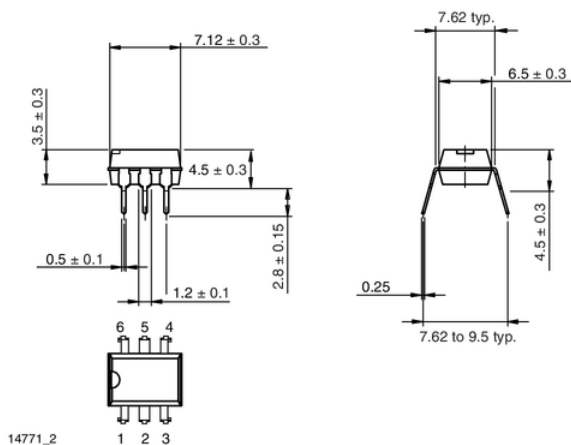
Fig. 13 - Switching Timing

4N35, 4N36, 4N37

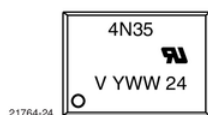
Vishay Semiconductors Optocoupler, Phototransistor Output,
with Base Connection



PACKAGE DIMENSIONS in millimeters



PACKAGE MARKING





Disclaimer

ALL PRODUCT, PRODUCT SPECIFICATIONS AND DATA ARE SUBJECT TO CHANGE WITHOUT NOTICE TO IMPROVE RELIABILITY, FUNCTION OR DESIGN OR OTHERWISE.

Vishay Intertechnology, Inc., its affiliates, agents, and employees, and all persons acting on its or their behalf (collectively, "Vishay"), disclaim any and all liability for any errors, inaccuracies or incompleteness contained in any datasheet or in any other disclosure relating to any product.

Vishay makes no warranty, representation or guarantee regarding the suitability of the products for any particular purpose or the continuing production of any product. To the maximum extent permitted by applicable law, Vishay disclaims (i) any and all liability arising out of the application or use of any product, (ii) any and all liability, including without limitation special, consequential or incidental damages, and (iii) any and all implied warranties, including warranties of fitness for particular purpose, non-infringement and merchantability.

Statements regarding the suitability of products for certain types of applications are based on Vishay's knowledge of typical requirements that are often placed on Vishay products in generic applications. Such statements are not binding statements about the suitability of products for a particular application. It is the customer's responsibility to validate that a particular product with the properties described in the product specification is suitable for use in a particular application. Parameters provided in datasheets and / or specifications may vary in different applications and performance may vary over time. All operating parameters, including typical parameters, must be validated for each customer application by the customer's technical experts. Product specifications do not expand or otherwise modify Vishay's terms and conditions of purchase, including but not limited to the warranty expressed therein.

Except as expressly indicated in writing, Vishay products are not designed for use in medical, life-saving, or life-sustaining applications or for any other application in which the failure of the Vishay product could result in personal injury or death. Customers using or selling Vishay products not expressly indicated for use in such applications do so at their own risk. Please contact authorized Vishay personnel to obtain written terms and conditions regarding products designed for such applications.

No license, express or implied, by estoppel or otherwise, to any intellectual property rights is granted by this document or by any conduct of Vishay. Product names and markings noted herein may be trademarks of their respective owners.

A.3 Instrumentational Amplifier and op amp datasheet

Table of Contents

1 Features	1	7.4 Device Functional Modes.....	11
2 Applications	1	8 Application and Implementation	12
3 Description	1	8.1 Application Information.....	12
4 Revision History	2	8.2 Typical Application	12
5 Pin Configuration and Functions	3	9 Power Supply Recommendations	16
6 Specifications	5	9.1 Low Voltage Operation	16
6.1 Absolute Maximum Ratings	5	10 Layout	17
6.2 ESD Ratings	5	10.1 Layout Guidelines	17
6.3 Recommended Operating Conditions.....	5	10.2 Layout Example	18
6.4 Thermal Information: INA126	5	11 Device and Documentation Support	19
6.5 Thermal Information: INA2126	6	11.1 Related Links	19
6.6 Electrical Characteristics.....	6	11.2 Community Resources.....	19
6.7 Typical Characteristics.....	8	11.3 Trademarks	19
7 Detailed Description	11	11.4 Electrostatic Discharge Caution	19
7.1 Overview	11	11.5 Glossary.....	19
7.2 Functional Block Diagram	11	12 Mechanical, Packaging, and Orderable Information	19
7.3 Feature Description	11		

4 Revision History

NOTE: Page numbers for previous revisions may differ from page numbers in the current version.

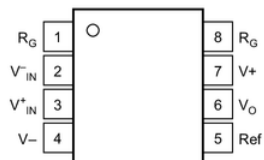
Changes from Revision A (August 2005) to Revision B

Page

- Added ESD Ratings table, Feature Description section, Device Functional Modes, Application and Implementation section, Power Supply Recommendations section, Layout section, Device and Documentation Support section, and Mechanical, Packaging, and Orderable Information section **1**

5 Pin Configuration and Functions

**P, D, and DGK Packages
8-Pin PDIP, SOIC, VSSOP
Top View**

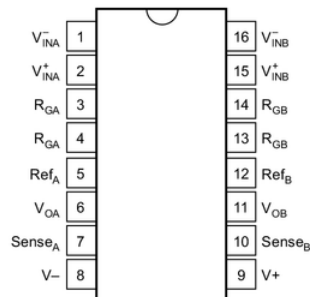


Pin Functions: 8-Pin

PIN		I/O	DESCRIPTION
NO.	NAME		
1, 8	R_G	—	Gain setting pin. For gains greater than 5 place a gain resistor between pin 1 and pin 8.
2	V_{IN-}	I	Negative input
3	V_{IN+}	I	Positive input
4	V_-	—	Negative supply
5	Ref	I	Reference input. This pin must be driven by a low impedance or connected to ground.
6	V_O	O	Output
7	V_+	—	Positive supply

INA126, INA2126

SBOS062B – SEPTEMBER 2000 – REVISED DECEMBER 2015

www.ti.com
**N, D, and DBQ Packages
16-Pin PDIP, SOIC, SSOP
Top View**

Pin Functions: 16-Pin

PIN		I/O	DESCRIPTION
NO.	NAME		
1	V_{INA}^-	I	Negative input for amplifier A
2	V_{INA}^+	I	Positive input for amplifier A
3, 4	R_{GA}	—	Gain setting pin for amplifier A. For gains greater than 5 place a gain resistor between pin 3 and pin 4.
5	Ref_A	I	Reference input for amplifier A. This pin must be driven by a low impedance or connected to ground.
6	V_{OA}	O	Output of amplifier A
7	$Sense_A$	I	Feedback for amplifier A. Connect to VOA, amplifier A output.
8	V^-	—	Negative supply
9	V^+	—	Positive supply
10	$Sense_B$	I	Feedback for amplifier B. Connect to VOB, amplifier B output.
11	V_{OB}	O	Output of amplifier B
12	Ref_B	I	Reference input for amplifier B. This pin must be driven by a low impedance or connected to ground.
13, 14	R_{GB}	—	Gain setting pin for amplifier B. For gains greater than 5 place a gain resistor between pin 13 and pin 14.
15	V_{INB}^+	I	Positive input for amplifier B
16	V_{INB}^-	I	Negative input for amplifier B

6 Specifications

6.1 Absolute Maximum Ratings

over operating free-air temperature range (unless otherwise noted) ⁽¹⁾

	MIN	MAX	UNIT
Power supply voltage, V+ to V–		36	V
Input signal voltage ⁽²⁾	(V–) – 0.7	(V+) + 0.7	
Input signal current ⁽²⁾		10	mA
Output short circuit		Continuous	
Operating temperature	–55	125	°C
Lead temperature (soldering, 10 s)		300	°C
Storage temperature, T _{stg}	–55	125	°C

(1) Stresses beyond those listed under *Absolute Maximum Ratings* may cause permanent damage to the device. These are stress ratings only, which do not imply functional operation of the device at these or any other conditions beyond those indicated under *Recommended Operating Conditions*. Exposure to absolute-maximum-rated conditions for extended periods may affect device reliability.

(2) Input signal voltage is limited by internal diodes connected to power supplies. See text.

6.2 ESD Ratings

	VALUE	UNIT
V _(ESD) Electrostatic discharge Human-body model (HBM), per ANSI/ESDA/JEDEC JS-001 ⁽¹⁾	±500	V

(1) JEDEC document JEP155 states that 500-V HBM allows safe manufacturing with a standard ESD control process.

6.3 Recommended Operating Conditions

over operating free-air temperature range (unless otherwise noted)

	MIN	NOM	MAX	UNIT
V+ V power supply	±135	±15	±18	V
V _O Input common mode voltage for V _O = 0		±11.25		V
T _A Operating temperature	–55		125	°C

6.4 Thermal Information: INA126

THERMAL METRIC ⁽¹⁾		INA126			UNIT
		PDIP	SOIC	MSOP	
		8 PINS	8 PINS	8 PINS	
R _{θJA}	Junction-to-ambient thermal resistance	52.2	116.4	167.8	°C/W
R _{θJC(top)}	Junction-to-case (top) thermal resistance	41.6	62.4	60.9	°C/W
R _{θJB}	Junction-to-board thermal resistance	29.4	57.7	88.9	°C/W
Ψ _{JT}	Junction-to-top characterization parameter	18.9	10	7.3	°C/W
Ψ _{JB}	Junction-to-board characterization parameter	29.2	57.1	87.3	°C/W
R _{θJC(bot)}	Junction-to-case (bottom) thermal resistance	–	–	–	°C/W

(1) For more information about traditional and new thermal metrics, see the *Semiconductor and IC Package Thermal Metrics* application report, [SPRA953](#).

INA126, INA2126

SBOS062B – SEPTEMBER 2000 – REVISED DECEMBER 2015

www.ti.com
6.5 Thermal Information: INA2126

THERMAL METRIC ⁽¹⁾		INA2126			UNIT
		PDIP	SOIC	MSOP	
		16 PINS	16 PINS	16 PINS	
R _{θJA}	Junction-to-ambient thermal resistance	39.3	76.2	115.8	°C/W
R _{θJC(top)}	Junction-to-case (top) thermal resistance	26.2	37.8	67	°C/W
R _{θJB}	Junction-to-board thermal resistance	20.1	33.5	58.3	°C/W
Ψ _{JT}	Junction-to-top characterization parameter	10.7	7.5	19.9	°C/W
Ψ _{JB}	Junction-to-board characterization parameter	19.9	33.3	57.9	°C/W
R _{θJC(bot)}	Junction-to-case (bottom) thermal resistance	–	–	–	°C/W

(1) For more information about traditional and new thermal metrics, see the *Semiconductor and IC Package Thermal Metrics* application report, [SPRA953](http://www.ti.com/lit/an/spra953/spra953.pdf).

6.6 Electrical Characteristics

at T_A = 25°C, V_S = ±15 V, R_L = 25 kΩ (unless otherwise noted)

PARAMETER		TEST CONDITIONS		MIN	TYP	MAX	UNIT
INPUT							
RTI	Offset voltage	NA126P, U, E; INA2126P, U, E			±100	±250	μV
		INA126PA, UA, EA; INA2126PA, UA, EA			±150	±500	
	Offset voltage versus temperature	NA126P, U, E; INA2126P, U, E			±0.5	±3	μV/°C
		INA126PA, UA, EA; INA2126PA, UA, EA			±0.5	±5	
	Offset voltage versus power supply (PSRR)	V _S = ±1.35 V to ±18	VNA126P, U, E INA2126P, U, E			5	15
VINA126PA, UA, EA INA2126PA, UA, EA				5	50		
Input impedance		INA126P, U, E; INA2126P, U, E			10 ⁹ 4		Ω pF
Safe input voltage		R _S = 0		(V-) - 0.5		(V+) + 0.5	V
		R _S = 1 kΩ		(V-) - 10		(V+) + 10	
Common-mode voltage range		V _O = 0 V		±11.25	±11.5		V
Channel separation (dual)		G = 5, dc			130		dB
Common-mode rejection		R _S = 0, V _{CM} = ±11.25 V	INA126P, U, E INA2126P, U, E	83	94		dB
			INA126PA, UA, EA INA2126PA, UA, EA	74	90		
		NA2126U (dual SO-16)		80	94		
INPUT BIAS CURRENT							
Input bias current		INA126P, U, E; INA2126P, U, E			-10	-25	nA
		INA126PA, UA, EA; INA2126PA, UA, EA				-50	
Input bias current vs temperature					±30		pA/°C
Offset current		INA126P, U, E; INA2126P, U, E			±0.5	±2	nA
		INA126PA, UA, EA; INA2126PA, UA, EA			±0.5	±5	
Offset current vs temperature					±10		pA/°C
GAIN							
Gain					G = 5 to 10k		V/V
Gain equation					G = 5 + 80 kΩ/R _G		V/V
Gain error		V _O = ±14 V, G = 5	INA126P, U, E INA2126P, U, E		±0.02%	±0.1%	
			INA126PA, UA, EA INA2126PA, UA, EA		±0.02%	±0.18%	
Gain error vs temperature		G = 5			±2	±10	ppm/°C
Gain error		V _O = ±12 V, G = 100	INA126P, U, E INA2126P, U, E		±0.2%	±0.5%	
			INA126PA, UA, EA INA2126PA, UA, EA		±0.2%	±1%	
Gain error vs temperature		G = 100			±25	±100	ppm/°C

Electrical Characteristics (continued)

at $T_A = 25^\circ\text{C}$, $V_S = \pm 15\text{ V}$, $R_L = 25\text{ k}\Omega$ (unless otherwise noted)

PARAMETER	TEST CONDITIONS	MIN	TYP	MAX	UNIT
Nonlinearity	$G = 100$, $V_O = \pm 14\text{ V}$		$\pm 0.002\%$	$\pm 0.012\%$	
NOISE					
Voltage noise	$f = 1\text{ kHz}$		35		$\text{nV}/\sqrt{\text{Hz}}$
	$f = 100\text{ Hz}$		35		
	$f = 10\text{ Hz}$		45		
	$f_B = 0.1\text{ Hz to } 10\text{ Hz}$		0.7		μV_{PP}
Current noise	$f = 1\text{ kHz}$		60		$\text{fA}/\sqrt{\text{Hz}}$
	$f_B = 0.1\text{ Hz to } 10\text{ Hz}$		2		pA_{PP}
OUTPUT					
Positive voltage	$R_L = 25\text{ k}\Omega$	$(V+) - 0.9$	$(V+) - 0.75$		V
Negative voltage	$R_L = 25\text{ k}\Omega$	$(V-) + 0.95$	$(V-) + 0.8$		
Short-circuit current	Short circuit to ground		$+10 / -5$		mA
Capacitive load drive			1000		pF
FREQUENCY RESPONSE					
Bandwidth, -3dB	$G = 5$		200		kHz
	$G = 100$		9		
	$G = 500$		1.8		
Slew rate	$V_O = \pm 10\text{ V}$, $G = 5$		0.4		$\text{V}/\mu\text{s}$
Settling time, 0.01%	10-V step, $G = 5$		30		μs
	10-V step, $G = 100$		160		
	10-V step, $G = 500$		1500		
Overload recovery	50% input overload		4		μs
POWER SUPPLY					
Voltage range		± 1.35	± 15	± 18	V
Current (per channel)	$I_O = 0$		± 175	± 200	μA
Specification temperature range		-40		85	$^\circ\text{C}$
Operation temperature range		-55		125	$^\circ\text{C}$

INA126, INA2126

SBOS062B—SEPTEMBER 2000—REVISED DECEMBER 2015

www.ti.com

6.7 Typical Characteristics

at $T_A = 25^\circ\text{C}$, $V_S = \pm 15\text{ V}$ (unless otherwise noted)

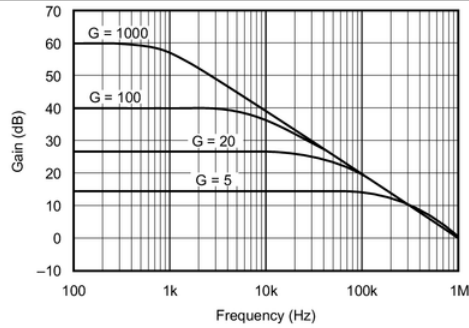


Figure 1. Gain vs Frequency

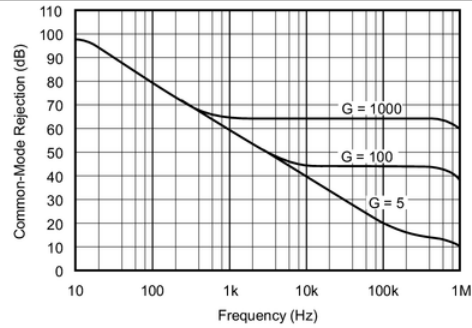


Figure 2. Common-Mode Rejection vs Frequency

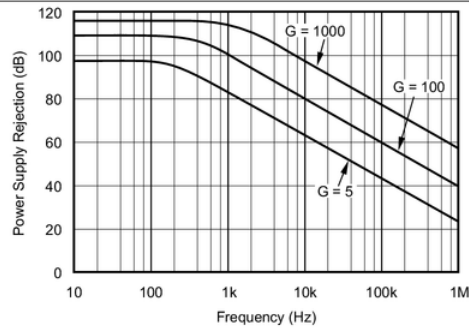


Figure 3. Positive Power Supply Rejection vs Frequency

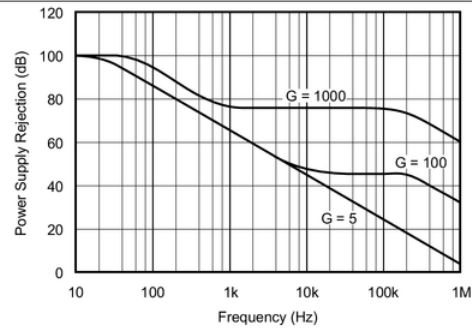


Figure 4. Negative Power Supply Rejection vs Frequency

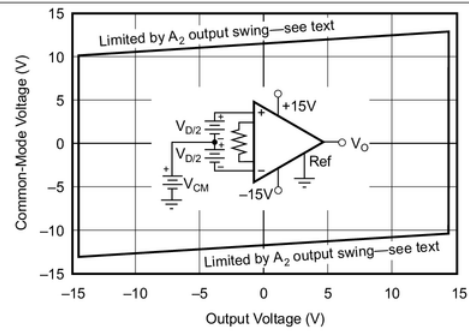


Figure 5. Input Common-Mode Range vs Output Voltage, $V_S = \pm 15\text{ V}$

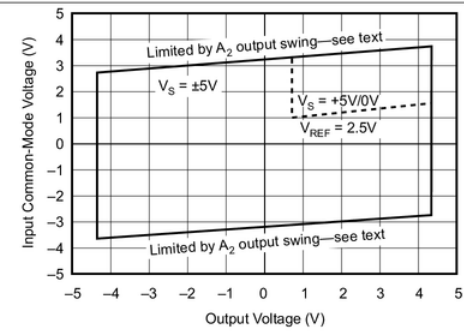


Figure 6. Input Common-Mode Voltage Range vs Output Voltage, $V_S = \pm 5\text{ V}$



Ultraprecision Operational Amplifier

Data Sheet

OP177

FEATURES

Ultralow offset voltage

$T_A = 25^\circ\text{C}$, 25 μV maximum

Outstanding offset voltage drift 0.3 $\mu\text{V}/^\circ\text{C}$ maximum

Excellent open-loop gain and gain linearity

12 $\text{V}/\mu\text{V}$ typical

CMRR: 130 dB minimum

PSRR: 115 dB minimum

Low supply current 2.0 mA maximum

Fits industry-standard precision operational amplifier sockets

GENERAL DESCRIPTION

The **OP177** features one of the highest precision performance of any operational amplifier currently available. Offset voltage of the **OP177** is only 25 μV maximum at room temperature. The ultralow V_{OS} of the **OP177** combines with the exceptional offset voltage drift (TCV_{OS}) of 0.3 $\mu\text{V}/^\circ\text{C}$ maximum to eliminate the need for external V_{OS} adjustment and increases system accuracy over temperature.

The **OP177** open-loop gain of 12 $\text{V}/\mu\text{V}$ is maintained over the full $\pm 10 \text{ V}$ output range. CMRR of 130 dB minimum, PSRR of 120 dB minimum, and maximum supply current of 2 mA are just a few examples of the excellent performance of this operational amplifier. The combination of outstanding specifications of the **OP177** ensures accurate performance in high closed-loop gain applications.

PIN CONFIGURATION

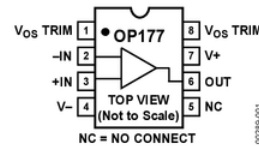


Figure 1. 8-Lead PDIP (P-Suffix),
8-Lead SOIC (S-Suffix)

This low noise, bipolar input operational amplifier is also a cost effective alternative to chopper-stabilized amplifiers. The **OP177** provides chopper-type performance without the usual problems of high noise, low frequency chopper spikes, large physical size, limited common-mode input voltage range, and bulky external storage capacitors.

The **OP177** is offered in the -40°C to $+85^\circ\text{C}$ extended industrial temperature ranges. This product is available in 8-lead PDIP, as well as the space saving 8-lead SOIC.

FUNCTIONAL BLOCK DIAGRAM

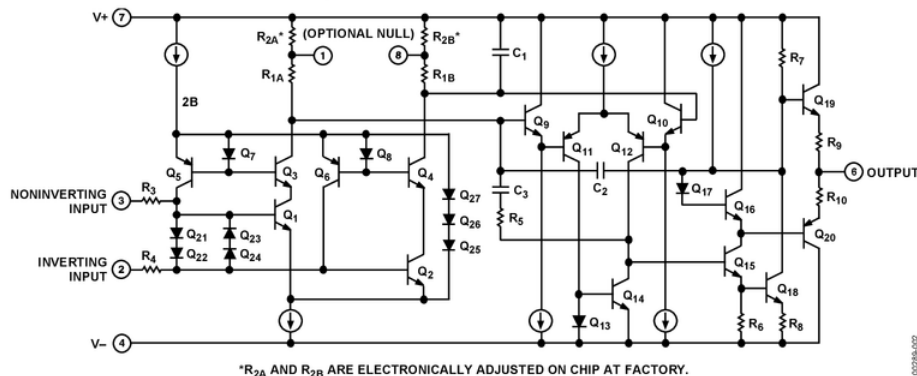


Figure 2. Simplified Schematic

Rev. H

[Document Feedback](#)

Information furnished by Analog Devices is believed to be accurate and reliable. However, no responsibility is assumed by Analog Devices for its use, nor for any infringements of patents or other rights of third parties that may result from its use. Specifications subject to change without notice. No license is granted by implication or otherwise under any patent or patent rights of Analog Devices. Trademarks and registered trademarks are the property of their respective owners.

One Technology Way, P.O. Box 9106, Norwood, MA 02062-9106, U.S.A.
Tel: 781.329.4700 ©1995–2016 Analog Devices, Inc. All rights reserved.
[Technical Support](#) www.analog.com

OP177* PRODUCT PAGE QUICK LINKS

Last Content Update: 06/09/2017

COMPARABLE PARTS

View a parametric search of comparable parts.

EVALUATION KITS

- EVAL-OPAMP-1 Evaluation Board

DOCUMENTATION

Application Notes

- AN-649: Using the Analog Devices Active Filter Design Tool

Data Sheet

- OP177: Ultraprecision Operational Amplifier Data Sheet

TOOLS AND SIMULATIONS

- OP177 SPICE Macro Model

REFERENCE DESIGNS

- CN0039
- CN0040
- CN0041
- CN0042
- CN0048
- CN0052
- CN0061

REFERENCE MATERIALS

Technical Articles

- High-Voltage Monitor Features High Accuracy

DESIGN RESOURCES

- OP177 Material Declaration
- PCN-PDN Information
- Quality And Reliability
- Symbols and Footprints

DISCUSSIONS

View all OP177 EngineerZone Discussions.

SAMPLE AND BUY

Visit the product page to see pricing options.

TECHNICAL SUPPORT

Submit a technical question or find your regional support number.

DOCUMENT FEEDBACK

Submit feedback for this data sheet.

This page is dynamically generated by Analog Devices, Inc., and inserted into this data sheet. A dynamic change to the content on this page will not trigger a change to either the revision number or the content of the product data sheet. This dynamic page may be frequently modified.

TABLE OF CONTENTS

Features	1
Pin Configuration	1
General Description	1
Functional Block Diagram	1
Revision History	2
Specifications.....	3
Electrical Characteristics.....	3
Test Circuits.....	4
Absolute Maximum Ratings.....	5
Thermal Resistance	5
ESD Caution.....	5
Typical Performance Characteristics	6

REVISION HISTORY

4/16—Rev. G to Rev. H	
Changes to Figure 27	9
9/12—Rev. F to Rev. G	
Changes to Features and General Description Section	1
Updated Outline Dimensions	13
Changes to Ordering Guide	14
3/09—Rev. E to Rev. F	
Added Figure 23, Renumbered Sequentially	8
Updated Outline Dimensions	13
5/06—Rev. D to Rev. E	
Changes to Figure 1	1
Change to Specifications Table 1	3
Changes to Specifications Table 2.....	4
Changes to Table 3.....	5
Changes to Figure 23 and Figure 24.....	9
Changes to Figure 32.....	12
Updated the Ordering Guide	14

Applications Information	9
Gain Linearity	9
Thermocouple Amplifier with Cold-Junction Compensation.....	9
Precision High Gain Differential Amplifier	10
Isolating Large Capacitive Loads.....	10
Bilateral Current Source	10
Precision Absolute Value Amplifier.....	10
Precision Positive Peak Detector	12
Precision Threshold Detector/Amplifier	12
Outline Dimensions	13
Ordering Guide	14

4/06—Rev. C to Rev. D	
Change to Pin Configuration Caption	1
Changes to Features	1
Change to Table 2	4
Change to Figure 2	4
Changes to Figure 10 and Figure 11	6
Changes to Figure 12 through Figure 17	7
Changes to Figure 18 through Figure 22	8
Change to Figure 27	10
Changes to Figure 30 and Figure 31	11
Updated Outline Dimensions.....	13
Changes to Ordering Guide	13

1/05—Rev. B to Rev. C	
Edits to Features.....	1
Edits to General Description	1
Edits to Pin Connections.....	1
Edits to Electrical Characteristics	2, 3
Global deletion of references to OP177E	3, 4, 10
Edits to Absolute Maximum Ratings	5
Edits to Package Type	5
Edits to Ordering Guide	5
Edit to Outline Dimensions	11

11/95—Rev. 0: Initial Version

SPECIFICATIONS

ELECTRICAL CHARACTERISTICS

At $V_S = \pm 15\text{ V}$, $T_A = 25^\circ\text{C}$, unless otherwise noted.

Table 1.

Parameter	Symbol	Test Conditions/Comments	OP177F			OP177G			Unit
			Min	Typ	Max	Min	Typ	Max	
INPUT OFFSET VOLTAGE	V_{OS}			10	25		20	60	μV
LONG-TERM INPUT OFFSET ¹									
Voltage Stability	$\Delta V_{OS}/\text{time}$			0.3			0.4		$\mu\text{V}/\text{mo}$
INPUT OFFSET CURRENT	I_{OS}			0.3	1.5		0.3	2.8	nA
INPUT BIAS CURRENT	I_B		-0.2	+1.2	+2	-0.2	+1.2	+2.8	nA
INPUT NOISE VOLTAGE	e_n	$f_0 = 1\text{ Hz to }100\text{ Hz}^2$		118	150		118	150	nV rms
INPUT NOISE CURRENT	i_n	$f_0 = 1\text{ Hz to }100\text{ Hz}^2$		3	8		3	8	pA rms
INPUT RESISTANCE									
Differential Mode ³	R_{IN}		26	45		18.5	45		M Ω
INPUT RESISTANCE COMMON MODE	R_{INCM}			200			200		G Ω
INPUT VOLTAGE RANGE ⁴	IVR		± 13	± 14		± 13	± 14		V
COMMON-MODE REJECTION RATIO	CMRR	$V_{CM} = \pm 13\text{ V}$	130	140		115	140		dB
POWER SUPPLY REJECTION RATIO	PSRR	$V_S = \pm 3\text{ V to } \pm 18\text{ V}$	115	125		110	120		dB
LARGE SIGNAL VOLTAGE GAIN	A_{VO}	$R_L \geq 2\text{ k}\Omega$, $V_O = \pm 10\text{ V}^5$	5000	12,000		2000	6000		V/mV
OUTPUT VOLTAGE SWING	V_O	$R_L \geq 10\text{ k}\Omega$	± 13.5	± 14.0		± 13.5	± 14.0		V
		$R_L \geq 2\text{ k}\Omega$	± 12.5	± 13.0		± 12.5	± 13.0		V
		$R_L \geq 1\text{ k}\Omega$	± 12.0	± 12.5		± 12.0	± 12.5		V
SLEW RATE ²	SR	$R_L \geq 2\text{ k}\Omega$	0.1	0.3		0.1	0.3		V/ μs
CLOSED-LOOP BANDWIDTH ²	BW	$A_{VCL} = 1$	0.4	0.6		0.4	0.6		MHz
OPEN-LOOP OUTPUT RESISTANCE	R_O			60			60		Ω
POWER CONSUMPTION	P_D	$V_S = \pm 15\text{ V}$, no load		50	60		50	60	mW
		$V_S = \pm 3\text{ V}$, no load		3.5	4.5		3.5	4.5	mW
SUPPLY CURRENT	I_{SY}	$V_S = \pm 15\text{ V}$, no load		1.6	2		1.6	2	mA
OFFSET ADJUSTMENT RANGE		$R_P = 20\text{ k}\Omega$		± 3			± 3		mV

¹ Long-term input offset voltage stability refers to the averaged trend line of V_{OS} vs. time over extended periods after the first 30 days of operation. Excluding the initial hour of operation, changes in V_{OS} during the first 30 operating days are typically less than 2.0 μV .

² Sample tested.

³ Guaranteed by design.

⁴ Guaranteed by CMRR test condition.

⁵ To ensure high open-loop gain throughout the $\pm 10\text{ V}$ output range, A_{VO} is tested at $-10\text{ V} \leq V_O \leq 0\text{ V}$, $0\text{ V} \leq V_O \leq +10\text{ V}$, and $-10\text{ V} \leq V_O \leq +10\text{ V}$.

At $V_S = \pm 15\text{ V}$, $-40^\circ\text{C} \leq T_A \leq +85^\circ\text{C}$, unless otherwise noted.

Table 2.

Parameter	Symbol	Test Conditions/Comments	OP177F			OP177G			Unit
			Min	Typ	Max	Min	Typ	Max	
INPUT									
Input Offset Voltage	V _{OS}			15	40		20	100	μV
Average Input Offset Voltage Drift ¹	TCV _{OS}			0.1	0.3		0.7	1.2	μV/°C
Input Offset Current	I _{OS}			0.5	2.2		0.5	4.5	nA
Average Input Offset Current Drift ²	TCI _{OS}			1.5	40		1.5	85	pA/°C
Input Bias Current	I _B		−0.2	+2.4	+4		+2.4	±6	nA
Average Input Bias Current Drift ²	TCI _B			8	40		15	60	pA/°C
Input Voltage Range ³	IVR		±13	±13.5		±13	±13.5		V
COMMON-MODE REJECTION RATIO	CMRR	V _{CM} = ±13 V	120	140		110	140		dB
POWER SUPPLY REJECTION RATIO	PSRR	V _S = ±3 V to ±18 V	110	120		106	115		dB
LARGE-SIGNAL VOLTAGE GAIN ⁴	A _{VO}	R _L ≥ 2 kΩ, V _O = ±10 V	2000	6000		1000	4000		V/mV
OUTPUT VOLTAGE SWING	V _O	R _L ≥ 2 kΩ	±12	±13		±12	±13		V
POWER CONSUMPTION	P _D	V _S = ±15 V, no load		60	75		60	75	mW
SUPPLY CURRENT	I _{SY}	V _S = ±15 V, no load		20	2.5		2	2.5	mA

¹ TCV_{OS} is sample tested.

² Guaranteed by endpoint limits.

³ Guaranteed by CMRR test condition.

⁴ To ensure high open-loop gain throughout the $\pm 10\text{ V}$ output range, A_{VO} is tested at $-10\text{ V} \leq V_O \leq 0\text{ V}$, $0\text{ V} \leq V_O \leq +10\text{ V}$, and $-10\text{ V} \leq V_O \leq +10\text{ V}$.

TEST CIRCUITS

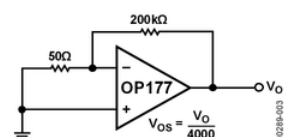


Figure 3. Typical Offset Voltage Test Circuit

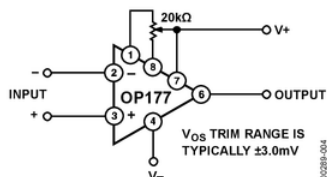


Figure 4. Optional Offset Nulling Circuit

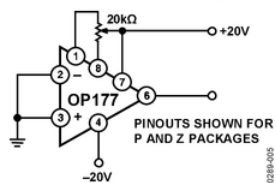


Figure 5. Burn-In Circuit

ABSOLUTE MAXIMUM RATINGS

Table 3.

Parameter	Ratings
Supply Voltage	± 22 V
Internal Power Dissipation ¹	500 mW
Differential Input Voltage	± 30 V
Input Voltage	± 22 V
Output Short-Circuit Duration	Indefinite
Storage Temperature Range	-65°C to $+125^{\circ}\text{C}$
Operating Temperature Range	-40°C to $+85^{\circ}\text{C}$
Lead Temperature (Soldering, 60 sec)	300°C
DICE Junction Temperature (T_J)	-65°C to $+150^{\circ}\text{C}$

¹ For supply voltages less than ± 22 V, the absolute maximum input voltage is equal to the supply voltage.

Stresses at or above those listed under Absolute Maximum Ratings may cause permanent damage to the product. This is a stress rating only; functional operation of the product at these or any other conditions above those indicated in the operational section of this specification is not implied. Operation beyond the maximum operating conditions for extended periods may affect product reliability.

THERMAL RESISTANCE

θ_{JA} is specified for worst-case mounting conditions, that is, θ_{JA} is specified for device in socket for PDIP; θ_{JA} is specified for device soldered to printed circuit board for SOIC package.

Table 4. Thermal Resistance

Package Type	θ_{JA}	θ_{JC}	Unit
8-Lead PDIP (P-Suffix)	103	43	$^{\circ}\text{C}/\text{W}$
8-Lead SOIC (S-Suffix)	158	43	$^{\circ}\text{C}/\text{W}$

ESD CAUTION



ESD (electrostatic discharge) sensitive device. Charged devices and circuit boards can discharge without detection. Although this product features patented or proprietary protection circuitry, damage may occur on devices subjected to high energy ESD. Therefore, proper ESD precautions should be taken to avoid performance degradation or loss of functionality.

TYPICAL PERFORMANCE CHARACTERISTICS

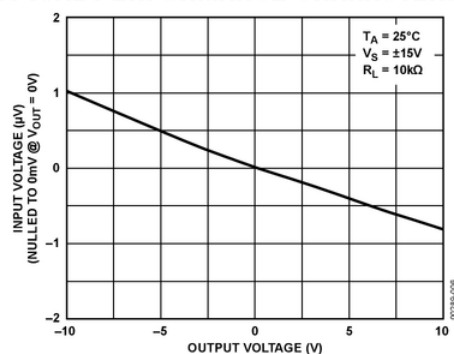


Figure 6. Gain Linearity (Input Voltage vs. Output Voltage)

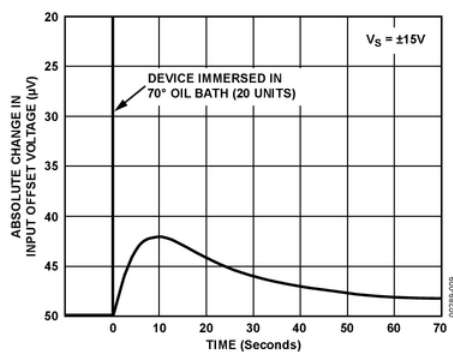


Figure 9. Offset Voltage Change Due to Thermal Shock

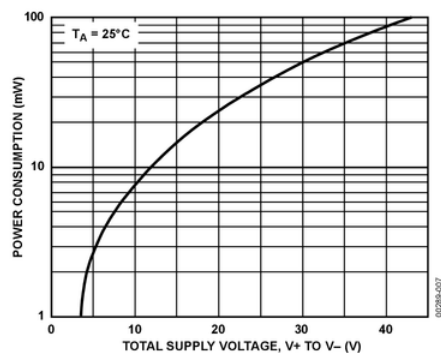


Figure 7. Power Consumption vs. Power Supply

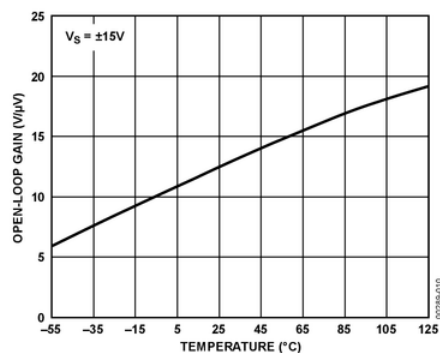


Figure 10. Open-Loop Gain vs. Temperature

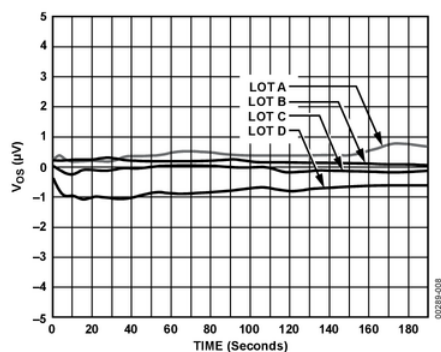


Figure 8. Warm-Up V_{os} Drift (Normalized) Z Package

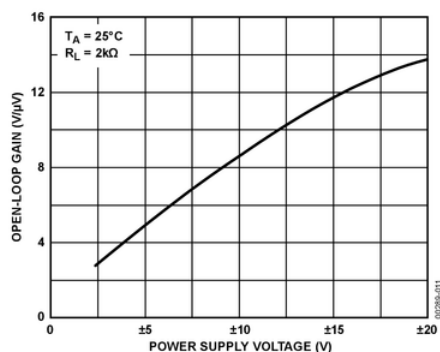


Figure 11. Open-Loop Gain vs. Power Supply Voltage











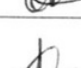

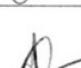






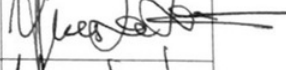




Appendix B

Project attendance form

B.1 Overview

This appendix contains the consultation meetings attendance form as required by the department. Both the supervisor and the student had to sign off the consultation meetings form for the official record of the meetings.

Consultation Meetings Attendance Form

Week	Date	Comments (if applicable)	Student's Signature	Supervisor's Signature
Week 1	03/08/17	Discussed on how to kick off my project		
Week 2	08/08/17	Had a discussion on where to find the parts which I was not able to find		
Week 3	15/08/17	Had a discussion on what to include in the project		
Week 4	22/08/17	Discussion on how to do the wiring and what to use		
Week 5	30/08/17	Discussion on what parts required for schematic		
Week 6	7/09/17	Week Discussed the design issues that I was having		
Week 7	15/09/17			
Week 8	22/09/17			
Week 9	29/09/17	Blended components, discussed possible solutions		
Week 10	5/10/17	coil not getting enough power, possible solution		
Week 11	12/10/17			
Week 12	30/10/17			

Bibliography

- [1] J. Mazaheri, H. Kamrani, F. Sareshtedari, and M. Fardmanesh, "Active magnetic field compensation system using proton precession scalar magnetometer for squid based applications," pp. 1378–1380, May 2015.
- [2] H. Liu, H. Dong, J. Ge, and B. Bai.
- [3] S. Hollos, *Signals from the subatomic world : how to build a proton precession magnetometer*. Longmont, CO: Abrazol Pub, 2008.
- [4] (2017) Magnetometer the history ct systems. [Online]. Available: <http://www.ctsystems.eu/support/magnetometer-the-history/>
- [5] P. T. Callaghan, C. D. Eccles, and J. D. Seymour, "An earths field nuclear magnetic resonance apparatus suitable for pulsed gradient spin echo measurements of self-diffusion under antarctic conditions," *Review of Scientific Instruments*, vol. 68, no. 11, pp. 4263–4270, 1997.
- [6] P. Mahavarkar, S. Singh, S. Labde, V. Dongre, and A. Patil, "The low cost proton precession magnetometer developed at the indian institute of geomagnetism," *Journal of Instrumentation*, vol. 12, no. 05, p. T05002, 2017. [Online]. Available: <http://stacks.iop.org/1748-0221/12/i=05/a=T05002>
- [7] X. Ping, Z. Shuang, and Shudong.
- [8] (2017) P-channel mosfet basics. [Online]. Available: <http://www.learningaboutelectronics.com/Articles/P-Channel-MOSFETs>
- [9] Wikipedia, "Eddy current — wikipedia, the free encyclopedia," 2017, [Online; accessed 22-October-2017]. [Online]. Available: https://en.wikipedia.org/w/index.php?title=Eddy_current&oldid=805268163
- [10] —, "johnsonnyquist noise — wikipedia, the free encyclopedia",."
- [11] —, "Q factor — wikipedia, the free encyclopedia," 2017, [Online; accessed 22-October-2017]. [Online]. Available: https://en.wikipedia.org/w/index.php?title=Q_factor&oldid=803869594
- [12] [Online]. Available: <http://www.abrazol.com/books/signals/#node.toc>